

THE SUITABILITY OF VERY LOW COST UNPILOTED AIRCRAFT  
SYSTEMS (UAS) FOR ENVIRONMENTAL SCIENCE RESEARCH

A Thesis submitted to the faculty of  
San Francisco State University  
In partial fulfillment of  
the requirements for  
the Degree

Master of Science

In

Geographic Information Science

by

Peter M. Christian

San Francisco, California

May 2015

Copyright by  
Peter M. Christian  
2015

## CERTIFICATION OF APPROVAL

I certify that I have read *The Suitability of Very Low Cost Unpiloted Aircraft Systems (UAS) for Environmental Science Research* by Peter M. Christian, and that in my opinion this work meets the criteria for approving a thesis submitted in partial fulfillment of the requirement for the degree Master of Science in Geographic Information Science at San Francisco State University.

---

Jerry Davis, Ph.D.  
Professor

---

Leonhard Blesius, Ph.D.  
Associate Professor

# The Suitability of Very Low Cost Unpiloted Aircraft Systems (UAS) for Environmental Science Research

Peter M. Christian

San Francisco, California

2015

The objective of this study is to evaluate the suitability of a very low cost unmanned aircraft system (UAS) for environmental science research. A small grant was obtained (<\$6500) to set up a complete UAS and to employ it to collect data in small montane meadows and hill slope gullies. The system comprises a 3D Robotics hexacopter, two Canon point-and-shoot cameras including one modified for near infrared (NIR) imagery. The collected data was used in an attempt to identify vegetation-obscured stream channels using NIR imagery and to calculate gully volume and erosion rates from digital surface models (DSM) created using Structure from Motion (SfM). The collected data was also compared against commonly used free data sources.

This research shows that using consumer grade cameras converted to multispectral sensors for detecting small, obscured montane meadow stream channels was unsuccessful but with further development has great promise. However, compared to the use of other imagery, the centimeter level resolution and low cost for rapid repeat visits by the UAS may justify their use in montane meadow stream monitoring. In the collection of gully data the resolution of the UAS derived SfM DSM can provide a precision for volumetric estimates substantially better than available public data. Additionally the ability to easily and cheaply repeat surveys and the fine resolution will make it possible to study erosion rates and estimate sediment yield through change in volume.

I certify that the Abstract is a correct representation of the content of this thesis.

---

Chair, Thesis Committee

---

Date

## ACKNOWLEDGEMENTS

This thesis would not have happened if it weren't for the support of my family and the assistance of many in the Geography department. I'd like to thank a few by name: Jerry Davis, Leo Blesius, Nancy Wilkinson, the denizens of the map library, Kate, David, the Joes, Garrett (the General) Bradford, William (dad) Christian, Zev Reuter, Erin Swan, and my roommates who put up with the noise of my flying contraptions. I'd also like to apologize to all the people in the Whole Foods cafe who wanted to sit down but couldn't because I was there for 8 hours straight day after day.

## TABLE OF CONTENTS

LIST OF TABLES _____	VII
LIST OF FIGURES _____	IX
INTRODUCTION _____	1
CHAPTER 1: UNPILOTED AERIAL VEHICLES (UAVS) _____	3
1.1 INTRODUCTION _____	3
1.2 SMALL UAV PLATFORM OPTIONS _____	7
1.3 THE SELECTION: A HEXACOPTER, THE GRANT AND THE PROJECT _____	9
CHAPTER 2: CAMERAS _____	9
2.1 INTRODUCTION _____	9
2.2 DIGITAL CAMERA TYPES _____	10
2.3 IMAGE CREATION _____	11
2.3.1 Pathway of Light to Image and Photodiodes _____	11
2.3.2 Signal Noise and ISO _____	12
2.2.3 Pixels, what are they? _____	13
2.2.4 Sensor Size Versus Megapixels _____	13
2.2.5 CMOS vs. CCD Sensors _____	14
2.2.6 Bayer Filters _____	15
2.2.7 Hotmirrors and Light Beyond the Visible Spectrum _____	16
2.2.8 Shutters and Shutter Speed _____	16
2.2.9 Aperture _____	17
2.2.10 Shutter Speed, Aperture, and ISO Balancing Act _____	17
2.2.11 Camera Settings Effects _____	17
2.3 DIGITAL IMAGE FORMATS _____	19
2.4 DCRAW AND IMAGEJ: GETTING IMAGES OF RAW DIGITAL NUMBERS _____	21
<a href="#">2.5</a> SHUTTER AUTOMATION AND CANON HACK DEVELOPMENT KIT (CHKD) _____	22
CHAPTER 3: THE NEAR INFRARED _____	25
3.1 INTRODUCTION: BEYOND THE VISIBLE SPECTRUM _____	25
3.2 FILTERS _____	26
3.3 NEAR INFRARED (NIR) _____	28
3.4 VEGETATION INDICES _____	30
3.5 SINGLE CAMERA VISIBLE/NIR PHOTOGRAPHY METHODS _____	32
3.6 SPECTRAL RESPONSE CURVE EXAMPLES: _____	35

3.7 SELECTED CAMERA:	36
CHAPTER 4: STRUCTURE FROM MOTION (SfM)	37
4.1 INTRODUCTION	37
4.2 SfM VERSUS LIDAR	38
4.3 ACCURACY	40
CHAPTER 5: MEADOWS	40
5.1 INTRODUCTION	40
5.2 PROBLEMS WITH STREAM IDENTIFICATION: SfM AND NIR APPROACHES	44
5.2.1 Results of SfM DEM Generation Using GoPro	44
5.3 MEADOW METHODS AND RESULTS:	45
5.4 RESULTS	49
CHAPTER 6: GULLIES	56
6.1 INTRODUCTION	56
6.2 STUDY SITE	58
6.3 METHODS	59
6.5 IMAGE PROCESSING RESULTS & ANALYSIS	61
6.6 DISCUSSION	64
CONCLUSION	69
REFERENCES	72

## List of Tables

Table 1. Consumer Camera Categories _____	11
Table 2. Camera Setting Effects _____	18
Table 3. Filter Types _____	27
Table 4. Consumer Camera Vegetation Indices_____	32
Table 6. Flight altitudes above ground level (AGL), ground sample distance (GSD), and overlap measured from photographs including in parentheses the number of photo pairs used in the measurements. _____	60
Table 7. Root-Mean Square Error (RMSE) estimates for models. _____	65
Table 8. Comparison of SfM and Golden Gate LiDAR Project DSMs. _____	66
Table 9. Volumetric and areal comparisons of SfM with USGS and GGLP DSMs. _____	68

## List of Figures

Figure 1. Images of a fan taken with: CCD sensor on the left and CMOS on the right.....	15
Figure 2. A Bayer color filter array with a RG1RG1/G2BG2B pixel arrangement.....	16
Figure 3. Uninterpolated raw pixels to image stack.....	22
Figure 4. Hoya’s filter transmission curves. ....	27
Figure 5. Behavior of light entering a modified and unmodified camera .....	29
Figure 6. Spectral response curves of 6 consumer cameras.....	36
Figure 7. NIR imagery of montane meadows (Loheide et al., 2009).....	42
Figure 8. Warped ground plane created from GoPro imagery.....	45
Figure 9. Dry Creek (left) and Knuthson Meadow (right) Area Maps .....	46
Figure 10. Knuthson flight plan on NIR mosaic.....	47
Figure 11. Dry Creek flight plan and way points.....	47
Figure 12. Example of the Mission Planner interface and Knuthson meadow flight plan. ....	48
Figure 14. Knuthson UAV Unmodified ‘CIR’ orthomosaic against satellite imagery.....	51
Figure 15. Knuthson UAV NDVI calculated for the same area overlaying the NAIP NDVI. ....	51
Figure 16. Knuthson NAIP NDVI .....	52
Figure 17. Dry Creek NAIP NDVI.....	52
Figure 18. Dry Creek UAV orthomosaic NDVI.....	53
Figure 19. The NAIP CIR image for the same area as figure 20.. ....	53
Figure 20. Dry Creek UAV single image displayed as 3-1-1 to better emulate CIR.....	54
Figure 21. Dry Creek NAIP NDVI individual image area.....	54
Figure 22. Dry Creek UAV single image NDVI. ....	55
Figure 23. Dry Creek 8a: unsupervised classification with 10 classes .....	55
Figure 24. Dry Creek 8b: unsupervised classification with 20 classes .....	56
Figure 25. Photograph taken from head of gully. ....	58
Figure 26. Three successive flight paths, with heights above launch pad of 10, 20 and 70 m. ....	61
Figure 27. Section of orthomosaic (originally in color) created from 20m flight.....	62
Figure 28. Digital Surface Model of 20m (33m average altitude AGL) Model. ....	63
Figure 29. Comparison of digital surface models.....	67

## **Introduction**

Most freely available aerial data has been provided by tax funded government institutions, or large commercial enterprises that profit from individuals accessing their data. Except for selected urban areas, these free data sets are of low spatial (>50cm) and/or temporal resolution (longer than yearly revisit rates). Additionally, free multispectral and elevation datasets are often of much poorer resolution. Researchers frequently need multispectral, 3D, and/or higher resolution data, but purchasing or gathering this data for specific scientific research purposes has traditionally been too expensive for many projects. The result is that researchers, especially student researchers, often choose study areas based on the availability of inexpensive, existing data sources rather than on preferred research goals. However, over the last 15 years, advances in radio controlled aircraft, robotics, digital cameras, and computer vision have enabled development of unpiloted aircraft systems (UAS) capable of collecting aerial 2D, 3D, and multispectral data at a more reasonable cost. While advances in UAS technology have come primarily from military applications, the advantages of using UAS for environmental science rather than on data distributed by corporations or governmental institutions has been recognized and is rapidly becoming more common (Bento, 2008).

Geomorphological and biogeographical science often needs more than 2 dimensional cartographic maps or aerial images. Research in these fields often requires 3 dimensional and multispectral data products in the form of raster DEMs from the USGS National Elevation Data set, field surveyed plan and longitudinal profiles, or aerial and terrestrial LiDAR point clouds. This data is needed to make volumetric measurements or to calculate spectral indices which can be used to model vegetation health, predict slope failure, or to determine sediment accumulation and loss.

Currently, conventional methods to acquire data at fine spatial or temporal resolution are expensive, either in person hours for field survey, or financially to purchase custom remote sensing products. Satellite and flight rentals are in the range of \$500 per collection session (<http://www.landinfo.com>). A lower cost method to collect 3D data will reduce the dependency of

researchers on preexisting or overly expensive datasets, allowing them to choose study areas based on their scientific importance rather than data availability.

Unpiloted aircraft systems (UAS), comprising an unpiloted aerial vehicle (UAV), sensors mounted on the UAV, a ground station to interface with the UAV, and equipment needed to maintain the UAV, have been available for some years, but it is only within the last decade that UASs have reached the consumer market. More significantly, it is only within the last 5 years that technological advances have brought the UAS within the typical non-grant university funding and the technical knowhow of non-engineers. However, products designed for consumer use such as those now available to non-engineers often pose risks of reduced and inadequate performance when compared to products designed for scientific use.

This study seeks to determine the feasibility of collecting and creating 2D, 3D, and multispectral datasets using a very low cost multirotor UAS and consumer point and shoot cameras. The paper first provides an introduction to UAS technology and options, including the selection of UAV and consumer digital camera options. The paper then describes the methods and results of the research on meadows and gullies, concluding with a final assessment of the utility of UAS-based data collection for geomorphological research.

We seek to answer whether a very low cost platform is capable of producing a grade of data usable by university researchers. We purchased a UAS and tested the system on two different research projects: to map stream channels in montane meadows in the Sierra Nevada in California and to create digital surface models of coastal hillslope gullies. The datasets produced were compared to similar, freely available data. We evaluate the strengths and weakness of the UAS collected data versus the free data based on the results of these study projects. The final objective was to determine if the UAS data is a suitable geomorphological research tool, and, if it is usable, what are the costs, benefits, and limitations of its use.

**UAV Choice:** Our early research on UAS indicated that we should select a multi-rotor UAV as the aircraft platform, based on flight characteristics and the body of prior research. Both indicated that multi-rotor aircraft (those aircraft with more than two rotors, e.g. quad-, hex-, and octocopters) might be a good choice for stream channel and gully survey because of their stability, reliability, and maneuverability.

**Camera Choice:** Camera choice was more complicated. Camera selection requires tradeoffs of weight, lens selection and data quality. Initially, we identified a high performance point and shoot camera to provide a good compromise between cost, weight, function, and image quality.

**Research Choice:** We chose two geomorphological topics that prove challenging to study using conventional methods as research areas: identifying small montane meadow stream channels and modeling hillslope gullies. The meadow stream channels, draining small watersheds of less than 30 km<sup>2</sup>, are very shallow and narrow (< 1.5 m), and often indistinguishable due to obscuring vegetation (Slocombe, 2014). Additionally, the stream channels are largely invisible in aerial imagery and are small enough to be indistinguishable in the available elevation datasets where stream widths are almost never greater than 1.5 meters and the highest resolution NED dataset is 3 meters. In order to model and monitor hillslope gullies one must be able to measure volumetric change. Readily available elevation data sets rarely capture all but the largest interior features of gullies, and their revisit rate is too slow to monitor seasonal change. The potential to capture very high resolution elevation and multispectral data at fast revisit rates make a UAV the optimal choice for the research of these two types of geomorphological features.

## **Chapter 1: Unpiloted Aerial Vehicles (UAVs)**

### **1.1 Introduction**

Both piloted and unpiloted aircraft have been used for scientific research. Selecting an Unpiloted Aerial Vehicle (UAV) rather than a piloted aircraft offers significant benefits to researchers; it increases safety by eliminating the chance of pilot and passenger injury in case of an aircraft accident and provides lower cost data with greater mission repeatability (Watts et al., 2012). An existing body of recent literature provides relevant information on selecting a UAV for research purposes. We survey first the advantages and problems with all types of UAVs for research, then narrow the options for small, low cost research projects such as the ones selected for this paper.

A number of authors have reported on the advantages of UAV based surveys. For example, Zongjian (2008) states his goal is finding a means to perform low altitude aerial photogrammetric surveys. His list of the advantages of using a UAV include the ability to record useful data on days when conditions like clouds and dust would prohibit the use of traditional platforms, i.e. satellites and manned aircraft, the ability to capture images of entire large buildings through complicated flight patterns, and the possibility of providing low cost and high temporal resolution photogrammetric products (Zongjian, 2008).

Laliberte et al. (2011) claim that the benefits of using a UAV versus traditional satellite imagery are that UAVs offer “the unique ability for repeated deployment for acquisition of high temporal resolution data at very high spatial resolution” and can record valid information in conditions where a satellite cannot. In their study, they noted that much of the satellite data used for comparison was obscured by clouds or dust.

Not all UAVs are created equal. There are nearly as many UAV choices as there are piloted vehicles. UAV technology is a rapidly evolving field, which results in some ambiguity in classifying UAVs. Hinkley et al. (2013), for example, list categories of UAV used by the US Air Force in an order primarily determined by flight duration and maximum altitude, ranging from extremely small, low power "micro" or "nano" aerial vehicles intended to be carried and launched by a single person to high-altitude long endurance vehicles that may exceed the size and abilities of piloted craft.

Watts et al. (2012) list several potential uses of UAVs and which categories best suit these uses. They indicate that vertical take-off and landing (VTOL) vehicles have several key advantages over more traditional aircraft. These include the portability of the vehicle and ability to operate without runways, making this platform a good candidate for remote and rugged environments. The ability to hover allows for observations that require loitering. The greater maneuverability of the craft also allows for missions in complex landscapes that prevent the straight line flight of fixed wing craft (Watts et al., 2012). However, the VTOL craft that many authors use are not within the budget of this project or most other similar research projects. For instance, the initial cost of the Draganflyer X6 hexacopter, a platform used by Nackaerts et al. (2010), exceeds \$15,000.

For tasks where lightweight sensors, shorter duration flights or smaller craft will suffice Watts et al. (2012) suggests that small fixed-wing craft are the better option. Similar to a VTOL craft, some fixed-wing UAV can operate without a formal runway, are low cost, and require a small operating crew. They exceed the ability of VTOL craft in terms of payload, flight time, and endurance. This is balanced by their limitations. Though they do not require a formal runway they need a long, clear, level surface on which to land, which is not always available in remote areas. However, increased flight times and distances often allow for takeoff and landing areas to be farther from the study area. Their most important disadvantage compared to VTOL craft is that they lack the maneuverability and hovering capability of VTOL (Watts et al. 2012).

Hinkley et al. (2013) note: “The potential user of UAS technology will need to take care in considering their data requirements which will drive the decision on which sensors are best to carry out their mission. Payload size, weight and power draw coupled with flight duration requirements and operational cost will largely determine the appropriate aircraft acceptable for the mission.” Ambrosia and Zajkowski (2012) opine that any sensor that can fit onto a UAV can fit onto a manned aircraft. They warn that money saved by using a UAV instead of a single pilot manned aircraft can often be negated by increased manpower costs when operating the UAV. Unlike a single pilot aircraft a UAV may require spotters, camera operators, and other assistants, and incur reductions in the accuracy of the final product due to sensor size limitations imposed by a UAV’s smaller size. Thus, it is essential to consider all factors influencing platform choice before making a decision, with a final decision made based on what will provide the desired outcome in the most efficient and effective way possible (Ambrosia & Zajkowski 2012).

Hinkley et al. (2013) identify two main challenges to the widespread use of UAVs, especially in populated areas. The first is the need for “sense and avoid” abilities on the unpiloted craft to ensure safety for other vehicles that may share airspace with the UAV. The second challenge is in communication with the UAV. In remote areas, few problems usually exist maintaining a clear radio frequency, however, in more populated areas, UAV communications share radio frequencies with other uses. The lack of a clear channel may inhibit the use of the UAV (Hinkley et al. 2012). These issues do not affect the research project in this paper, which was carried out in a remote environment.

A third issue affecting UAV use is determining accurate positioning. In an analysis of the use of a mini UAS as sensor platforms, Watts et al. (2012) note that position accuracy problems can limit the precision of the results. They state that until more accurate positioning technology is available, ground control points (GCP) will be needed. This is not a major stumbling block for our project and some similar research projects because the small size of the study area makes the placement of GCPs, usually a time consuming process, practical. However, this obstacle will be faced by projects covering larger areas (Watts et al. 2012).

Though not expressly an operational problem (and not a problem for this project), regulations of government bodies such as the US Federal Aviation Administration (FAA) can be an impediment to UAV based research. Non-exempt UAV flights in civil airspace in the US require a Certificate of Authorization (COA) issued by the FAA. For public university research, Experimental Category Certificates are available for larger UAV flights. However, as of late 2014 few of these (<200) have been issued, and it is not clear how many applicants have been rejected, so the percent of applicants that receive a certificate or are rejected is unknown. The certificate of airworthiness requires “a project aviation safety plan on how to mitigate the risk associated with operation of a UAS for a very specific location...” The certificate approval process can take up to 60 days, though the process is reportedly being streamlined. Accordingly, last minute projects are difficult to accommodate. However, once a certificate has been obtained, extensions or modifications of the approved area can be rapidly issued (Ambrosia & Zajkowski, 2012). In February, 2012, a bill originating in the US House of Representatives entitled “The FAA Modernization and Reform Act of 2012” became federal law. This law will help clarify regulations regarding UAV operations, with the intent of integrating UAV into the national airspace (Hinkley et al., 2012).

Aircraft considered hobby-grade remote controlled vehicles are currently exempted from the certificate process. The FAA has released guidelines but not promulgated regulations regarding their use. These guidelines include maintaining line of site with the aircraft, not operating above 400’, and not operating within restricted airspace such as near airports. The research project we conducted fell under the hobby-grade exemption. However, future use of UAVs for research may require complying with the certification process because the recently passed law will undoubtedly impose more stringent conditions on UAV flights. For example, the

FAA has proposed to regulate UAS with a takeoff weights between 2kg and 25kg. This 2kg lower weight limit may mean that many more research programs will soon need to obtain permits (Watts et al., 2012).

## **1.2 Small UAV Platform Options**

Budget and legal considerations for most university research projects necessitate the use of small UAVs, sometimes called sUAVs or mUAVs where the ‘m’ stands for micro, that operate at low altitudes. Researchers using vehicles in this category make use of a variety of aircraft that include both motorized and non-motorized platforms. Non-motorized platforms are a ‘low-tech’ option that have some advantages over motorized platforms. Gliders, balloons and other tethered craft can have greater payload capacity and endurance capabilities than small motorized aircraft, but are limited in their maximum altitude and maneuverability due to their dependence on a ground tether. Lighter-than-air UAV are also weather dependent, and the overhead obstruction of a balloon can make using GPS for navigation difficult.

The main benefits of non-motorized craft are larger payload capacity, mechanical simplicity, and potentially cheaper total cost. Kites are more stable in windy conditions than all other platforms, however, the platform is useless without a consistent wind, and the strength of the wind dictates payload capacity. Balloons and blimps have the capability to carry large payloads for a virtually unlimited time. However, significant wind makes the platform unusable. A helikite, a helium balloon with kite wings, is a compromise between the two. The balloon part can lift a payload in windless conditions. In windy conditions the kite part stabilizes the balloon and increases the payload capacity. The cost of these platforms, especially kites, is extremely low (Verhoeven et al., 2009; Verhoeven, 2009).

The disadvantage of non-motorized craft is that they are dependent on a ground attachment or tether, to either a person or to a stationary object. Moving a ground platform requires a path clear of overhead obstructions like trees and power lines and severely limits the maximum altitude of the platform. It is also difficult to record imagery along a precise path or to accurately position the camera. In addition, topography and wind direction are limiting factors. Non-motorized craft are well suited for general photography and long-term monitoring

applications but do not fulfill the needs of our project, which required controlled and accurate maneuvering over terrain, and were thus eliminated (Verhoeven, 2009).

Small motorized platforms provide advantages, including the freedom from a ground tether, accurate navigation, and higher distance and altitude limits. The disadvantages, mentioned previously, are smaller payloads, relative instability in windy conditions, and shorter flight time. Writing in 2009, Verhoeven stated that multi-rotor craft had great promise for research purposes, but were limited in size and were expensive, but he predicted a drop in price and an increase in size and payload capacity. In less than a decade, that prediction has come true: advances in UAV technology and lower prices allowed us to obtain and use a small multi-rotor craft in the project (Verhoeven, 2009).

A comparison of fixed wing craft and single rotor craft (i.e., helicopters) confirms that rotor craft have much greater maneuverability and can operate much closer to the ground but have lower payload limits, shorter flight times, tend to be more complex in their operation and mechanics, and are less stable. Many of these single rotor UAV limitations can be counteracted by using multi-rotor craft. These craft have 3 or more rotors, making them easier to fly, more stable, and able to carry greater payloads. And because there is redundancy in rotors, multi-rotors can be much more resistant to crashes caused by engine failure (Eisenbeiß, 2009).

Eisenbeiß (2009) performed critical research comparing autopilot versus human controlled multi-rotor flight. He concluded that in all conditions the use of an autopilot resulted in superior flight control, testing the stability of the craft, and recording the output from the onboard Inertial Measurement Unit (IMU). The autopilot's ability to stabilize the craft far exceeded that of the human pilot in both high-wind and calm conditions in all aspects of flight, including vehicle orientation (pitch, yaw) and horizontal and vertical hold. The stability of the craft is an essential aspect of aerial photography. This is especially true when using a camera in low light or with filters that may require longer exposure times. Without a stationary, stable platform the images will be blurry and potentially unusable (Eisenbeiß, 2009).

### **1.3 The selection: a hexacopter, the grant and the project**

Based on a careful evaluation of the studies and evidence outlined above, we decided that a 6-rotor hexacopter was the optimal platform, providing a balance of stability, reliability, maneuverability, and low cost. Based on a review of literature and our research needs, we sought and were awarded a grant of \$6500 from the Center for Computing for Life Sciences through the Geography & Environment Department at San Francisco State University. The grant allowed us to acquire and instrument a UAS and then evaluate it as a tool for a diverse range of geomorphological and other research. The system we used comprises a 3D Robotics hexacopter, Ardupilot automated flight hardware and software, spare parts and tool kit, two s95 Canon point-and-shoot cameras, including one modified for near infrared imagery, and a field laptop for mission planning. We also acquired a flight simulator and a Blade MQx mini quadcopter for pilot training and a license for Agisoft's Photoscan, a commercial software package tailored for aerial photogrammetry. We used this system successfully for geomorphic research in degraded and restored montane meadows to study stream channel formation using both visible and near infrared imagery. We also used the UAS for the creation of digital elevation models of large hillslope gullies using structure from motion (SfM) a method to mosaic images and derive digital surface models using consumer-grade digital cameras ([www.agisoft.ru](http://www.agisoft.ru); <http://www.3drobotics.com>; <http://www.maxmax.com>).

## **Chapter 2: Cameras**

### **2.1 Introduction**

Aerial photography using a small UAV makes lightweight cameras a priority, however, images used for research require a high level of quality. Very low cost point and shoot cameras with a retractable lens are often the lightest weight option but produce unacceptably lower quality images. More expensive, heavier cameras, such as digital single lens reflex cameras (DSLRs), produce higher quality images but the added weight usually makes them unsuitable for mounting on a small UAV. Cameras with interchangeable lenses increase image quality while adding cost and weight and may be a preferred option for UAV research.

Currently there is a vast array of consumer cameras for every budget, but few low-cost cameras are designed specifically for scientific research. Specialty research cameras, including large format, metric cameras for high altitude photogrammetry and multispectral/hyperspectral cameras, cost far more than the most expensive consumer cameras. However, methods exist to replace expensive professional cameras with much less expensive consumer cameras. We suggest reasonably priced cameras for UAV-mounted low-altitude aerial photography and camera settings and functions in the context of capturing images for research rather than for artistic purposes, including the mechanics of the image capture process that are affected when the camera is mounted on a UAV. The section will finish by discussing the use of digital cameras converted to capture multispectral data.

## **2.2 Digital Camera Types**

The quality of an image (crispness, color, and presence or absence of errors) is largely determined by the quality of a camera's lens and the size of its sensor (Curtin, 2007). As a general rule, larger sensors and more expensive lenses offer superior quality. Camera design is often separated into two main groups based on the intended use and the user, which determines the sensor size and lens. The first group—point and shoot cameras—is intended for beginner photographers who desire a very portable, easy to use, inexpensive camera. These are small cameras, the vast majority weighing less than a pound and usually less than half that. They have a fixed lens, small sensors, and usually cost less than \$500. Most of these cameras will fit into a pocket.

The other main group—digital single lens reflex cameras (DLSRs)-- places greater importance on quality of image and more feature and function options, sacrificing price and portability. DLSRs have larger sensors, a variety of interchangeable lenses, and the operation of the camera's settings (focus, aperture, shutter speed, ISO) can be manually adjusted. The cost of the cheapest of these cameras is currently about \$500 (Curtin, 2007).

There are two sub categories, both offering compromises between the simplicity of point and shoot cameras and the weight and complexity of DLSRs. These cameras fit more closely with UAV research purposes. The two subcategories are large sensor format point-and-shoots, which

move toward DSLR quality and functionality, and mirrorless interchangeable lens cameras, which provide some of the size and weight advantages of point-and-shoots.

Large format point-and-shoot cameras increase image quality and functionality over their smaller-sensor cousins. Most of their settings can be switched to manual mode, the lens is fixed but higher quality and the sensor is larger but still far from a full 35mm equivalent. Mirrorless interchangeable lens cameras are similar to their larger siblings but by simplifying the viewfinder, (mirrorless refers to how the viewfinder mechanism operates), and paring down functions and features, the size and weight of the camera is much reduced. These often appear to be point and shoot camera bodies with a DSLR lens affixed (Aber et al., 2010). These categories are summarized in the table below (Table 1).

Camera type	fixed lens	user	weight (1=lightest)	features/ options (1=fewest)	sensor size (1=smallest)	price (1=cheapest)
point and shoot (P&S)	y	less experienced	1	1	1	1
larger format P&S	y	more experienced	2	2	2	2
Mirrorless interchangeable lens	n	more experienced	3	3	3	3
DSLR	n	more experienced	4	4	4	4

Table 1. Consumer Camera Categories

## 2.3 Image Creation

### 2.3.1 Pathway of Light to Image and Photodiodes

The pathway of a single recorded photon from a light source to a display device is as follows. A photon enters the camera's lens, passes through a series of filters and hits the underlying sensor where it is counted (Adams et al., 1998; Curtin, 2007). A camera's sensor is made up of an array of photon collectors, or photodiodes. The output of a photodiode is a digital

number related to the count of the number of photons collected at that site. Each of these photodiodes is considered a pixel for a camera model's megapixel specification. Above the photodiodes lies a Bayer Color Filter Array (CFA). Each photodiode is covered by a red, green, or blue filter. In this way, a single photodiode records one color. The digital numbers from the sensor are interpreted and interpolated by the camera's software and an image is exported. A monitor's pixel value is based on the values stored in this image (Adams et al., 1998; Curtin, 2007; Fraser, 2004; Kawamura, 1998).

### **2.3.2 Signal Noise and ISO**

All photodiodes record a certain number of false positives. These false positives are called noise. An example of this can be seen when a picture is taken in total darkness. Not all photodiodes will return a photon count of zero. These non-zero error values are the noise inherent in the image capture system. Another example of noise (and likely the etymological root) comes from audio equipment. If you turn up a radio all the way with no music playing you will hear a hiss. This is the noise (literally, in this case) inherent in the equipment. Noise is random, making it nearly impossible to remove from an audio signal or from an image after a picture has been taken. Improvements in technology have decrease the amount of noise in photographic images. A single camera operating in a defined environment produces noise that is fairly constant and which is related to the sensitivity of the sensor. The sensitivity of the sensor to light is measured by a value called an ISO number. Higher numbers indicate greater sensitivity: an ISO of 200 means that the sensor is twice as sensitive to light as an ISO value of 100. ISO values can be varied in most cameras, and increasing the ISO number is a way to compensate for less light hitting the sensor. By adjusting the ISO acceptable images can be taken at faster shutter speeds or in lower light environments. In the case of cameras deployed on UAVs, reduced light is often the result of increasing the shutter speed or decreasing aperture, both of which are steps taken to compensate for camera movement. Increasing the ISO value, however, increases the levels of noise in the image. As sensor sensitivity is increased by boosting the ISO value the amount of noise relative to the amount of signal goes up. Returning to the radio example, turning up the volume produces a louder hiss at the same rate as the music volume increase. The ratio of music

to hiss remains the same across the volume spectrum, so, while hiss may be acceptable at very low volumes, as the volume increases the music will be accompanied by a more noticeable—and annoying-- level of hiss. Similarly, for camera images, images taken in low light with a high ISO lose crispness. Increasing the ISO value allows pictures to be taken in faint light but the image noise is more noticeable. This is why images taken in low light appear to be ‘grainy’ (Aber et al., 2010; Curtin, 2007; Kawamura, 1998).

### **2.2.3 Pixels, what are they?**

In cameras, pixels represent photodiodes. As noted above, they record light. Collectively, the megapixel count refers to each camera’s unique photodiode characteristics and numbers.<sup>1</sup> The ideal camera would be one that individually recorded every photon entering its lens. However, because that is physically impossible, real cameras must average a number of these photons. The closer the number of photodiodes comes to matching the number of entering photons, the less averaging has to be done. Additionally, the fewer photons that reach a photodiode the less sharp the image will be because of the effect of noise. Smaller photodiodes record fewer photons. This means that if all camera details are equal and light is limited, larger photodiodes will produce a better picture even if the resolution is lower (Aber et al., 2010; Bosak, 2012; Curtin, 2007; Fraser, 2004).

### **2.2.4 Sensor Size Versus Megapixels**

An often used specification for a camera is its pixels (the count of a sensor’s photodiodes). Although this is an important number, it is not the most important factor determining image quality. A better measurement of image quality is the combination of pixels and sensor size. Comparing two hypothetical cameras with the same number of pixels but different sensor sizes illustrates this phenomenon. Camera A is a point and shoot with a sensor size of 1 cm x 1 cm. Camera B is a professional DSLR with a sensor size of 2 cm x 2 cm. Each

---

<sup>1</sup> Pixels in other settings refer to screen resolution—for example in computer and television screens—or when the camera plays back recorded images on an internal or external screen. A pixel on a screen emits light, a pixel—photodiode-- on a camera sensor, records light.

sensor has 16 megapixels. Obviously the size of the pixels/photodiodes for camera A will be much smaller than for camera B. 16 megapixels are crammed onto one centimeter of sensor in camera A. Camera B will have only four megapixels per centimeter of sensor. Since larger photodiodes can capture more photons per image than smaller ones, they increase the sensitivity to light without relying on increasing the ISO value, which creates much less noise, contributing to higher quality images. When using a UAV, larger photodiodes, products of a larger sensor, allow faster shutter speeds and exposures without relying on increasing the ISO. Moreover, technical changes have improved photodiode performance in greater light sensitivity and lower noise levels. Thus, when comparing camera specifications it is important that the models are similar in age to avoid purchasing older, lower quality equipment (Aber et al., 2010; Bosak, 2012; Curtin, 2007; Neumann, 2008).

#### **2.2.5 CMOS vs. CCD Sensors**

Complementary metal oxide semiconductor (CMOS) and Charge-Coupled Device (CCD) are two different types of camera sensor. CCD sensors were developed before CMOS sensors. CCDs require specialized manufacturing technology, and inside the camera image processing components are separated from the photodiodes. CMOS sensors can be manufactured with the same machines that produce other computer microprocessors. This greatly reduces their cost and allows image processing components to be integrated into the sensor. This type of sensor is found in cellphones and other mobile devices as well as most cameras now on the market. When first introduced, the quality of CMOS sensors was inferior to CCDs. However, the two sensor types are now approximately equal for most photographic uses so very few camera manufacturers offer cameras with the more expensive CCD sensors. Though CMOS sensors have largely replaced CCD sensors, some differences between the two bear mentioning. The main advantage of CMOS sensors, besides their lower cost, is that they are much more energy efficient. The cost and energy efficiency advantages have led to their market supremacy. On the other hand, CCDs produce less noise, so they are better at producing crisp images in low light. In addition, cameras with CCD sensors have a shutter system that works better for capturing images while the subject or the camera is in motion. An understanding of the different shutter mechanisms is important because

of the effect on images of subjects taken while they are in motion. CCD sensors use a global shutter. CMOS sensors use a rolling shutter. The names accurately represent the chips' shutter processes. A global shutter gathers the photon counts from all photodiodes for the entire sensor at one time. Then the photodiodes photon count is reset and the process is begun again. A rolling shutter gathers photon counts one row of photodiodes at a time, 'rolling' across and down the sensor. Using the rolling shutter to take pictures of objects in motion or while the camera is in motion can produce errors. A good example of this is an image of rotating fan blades, where the CMOS shuttering does not accurately capture the moving blade (Figure 1).

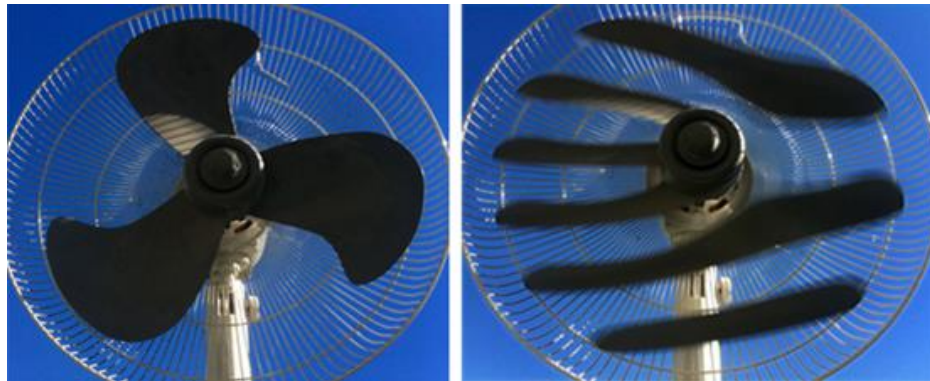


Figure 1. Images of a fan taken with: CCD sensor on the left and CMOS on the right. (<http://www.digitalbolex.com/global-shutter/>)

Aerial photography often involves movement of the camera due to both motor vibration and travel of the aircraft. An increase of the shutter speed can overcome this motion problem in many situations, but, in low light conditions, such as when using a filter, it may not be possible to increase shutter speeds. These two factors, motion and low light, hit at the Achilles' heel of CMOS sensors. Thus, when considering the choice of a camera for capturing images and for mounting on a UAV, CCD sensors may still be a better choice (Litwiller, 2001; Valentin et al., 2005).

### 2.2.6 Bayer Filters

Bayer Color Filter Arrays (CFA) help determine the wavelength that reaches each individual photodiode (Figure 2). They consist of red, green, and blue filters, with one color lying

above a single photodiode. The colors are alternated but there are twice as many green filters as red or blue. This distribution of twice as many green photodiodes as red or blue makes use of the human eye's greater sensitivity to green light to display light intensity information in addition to color information in the green channel (Fraser, 2004; Kawamura, 1998; Rabatel et al., 2012; Verhoeven, 2008).

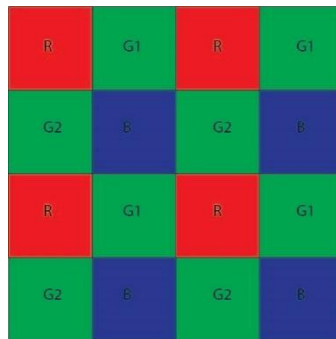


Figure 2. A Bayer color filter array with a RG1RG1/G2BG2B pixel arrangement

### 2.2.7 Hotmirrors and Light Beyond the Visible Spectrum

To counter the unwanted influence of wavelengths beyond visible light on images, camera manufacturers customarily install a filter in front of the sensor. This filter allows only visible light to hit the sensor, blocking both ultraviolet (UV) and near infrared (NIR) wavelengths. The removal of this filter is a necessary first step in converting a consumer grade camera to record NIR images (Adams et al., 1998; Rabatel et al., 2012; Rabatel et al., 2011; Verhoeven, 2008).

### 2.2.8 Shutters and Shutter Speed

The camera's shutter speed determines the amount of time the sensor is exposed to light, which controls the total amount of light that is recorded. Increasing shutter speed decreases the amount of light that reaches the sensor. Slowing the shutter speed does the opposite. In low light conditions, the shutter speed must be decreased to allow more light to be captured. If the camera or subject is in motion, the shutter speed must be increased to avoid blur. Because a UAV is subject to high degrees of motion, the fastest available shutter speed is often the best choice--but

this must be balanced against available light which may be limited if using filters or if other environmental conditions limit light (Aber et al., 2010; Bosak, 2012; Curtin, 2007).

### **2.2.9 Aperture**

Aperture is the size of the shutter opening which also helps determine the total amount of light that is recorded. Aperture also helps to determine the depth of field. Depth of field is the range of distance from the camera that is in focus. When performing low altitude aerial photography over terrain with high relief, it is especially important that the images have a deep depth of field. This will ensure that both high and low elevation features are simultaneously in focus. Narrowing the aperture increases the depth of field (Aber et al., 2010; Bosak, 2012; Curtin, 2007).

### **2.2.10 Shutter Speed, Aperture, and ISO Balancing Act**

To achieve a crisp image with a deep depth of field one must find a balance between these three settings. Because the UAV is in motion, a fast shutter speed is important. It is also important to use a low ISO setting, because this will result in non-grainy, crisp images. Additionally, a deep depth of field is important to keep the entire range of subjects in focus, so a smaller aperture should be used. All of these settings reduce the light available to the sensor. Usually some field testing must be done to determine which of these settings can or must be sacrificed to produce the best possible images (Aber et al., 2010; Bosak, 2012; Curtin, 2007).

### **2.2.11 Camera Settings Effects**

Table 2 summarizes the effects of camera settings on images and how changes to the setting will affect image quality.

factor	positive effect	negative effect
aperture (f-stop)	smaller apertures increase depth of field a greater range of objects will be in focus	a smaller aperture will decrease the amount of light hitting the sensor
shutter speed (fractions of seconds)	faster shutter speeds will decrease the blurring effect of a camera or subject in motion	faster shutter speeds decrease the amount of light hitting the sensor
auto focus	subject will be crisp at any distance from camera	using auto focus increases time between shots
manual focus	no time or power needed to focus between shots fast image capture	subject must be in a known distance from camera best used with 'infinite' focus or with a pole of known height
sensor size: "fractions of inch"	larger sensors increase image resolution because there are more pixels per feature	large sensors cost more and can decrease depth of field
photodiode size (sensor size/number of pixels)	larger photodiodes are more sensitive to light better images with less noise	larger photodiodes mean fewer photodiodes per sensor
photodiode density (number of pixels/sensor size)	higher density of photodiodes (more megapixels per sensor size) produce higher resolution images	higher densities mean smaller photodiodes which can produce noisier images and do not work well in low light
ISO (photodiode sensitivity)	low ISO produces less noisy images	much more light is needed when using a low ISO
focal length	a shorter focal length reduces effects of motion, increases light hitting sensor, increases depth of field	shorter focal length creates greater parallax at edges of image decrease relative size of features.

Table 2. Camera Setting Effects

### 2.3 Digital Image Formats

Common digital image formats include jpeg, tiff and raw, representing a progressive increase in stored information, and, depending on how the images are processed, a decrease in the modification of the original sensor data through post-processing by the camera's internal software. Collecting data in the raw format offers benefits when using a camera for scientific research. The capability to access the image data as recorded directly from the sensor is essential when a consumer camera is used for this purpose. Image based research and general photography have different requirements for photographs. General photography usually requires images to be aesthetically pleasing. Image-based research requires images to be accurate representations of the data being recorded. When image-based research involves an analysis of spectral signatures, such as calculating vegetation indices, the closer the image represents the sensor's photon count, the better. Post processing this sensor data of the image to make it suitable for viewing is a complex process; performing the image processing manually or in a knowledgeable way -- rather than letting the camera's proprietary onboard algorithm take care of the work -- is the only way to be sure that a consistent and accurate product suitable for research is obtained.

The camera-controlled image formats modify the data captured by the camera, sometimes substantially. Jpegs are images derived from the original sensor data, but are optimized to be aesthetically pleasing, and efficiently stored. Each channel is 8 bits, which can store 255 different possible values. The use of jpeg image format leads to a great reduction in the volume of information from the originally recorded data. The compression method and limited tonal values also decrease the accuracy and precision of the information. When converting from the base sensor digital numbers to a jpeg a number of modifications are usually made: lossy compression, demosaicing, devignetting, white balance, lens distortion correction, sharpening, noise reduction, and gamma correction. Each of these operations changes the original sensor values. Tiff, a second, lossless alternative format, is also designed to optimize the original sensor data for aesthetics and storage but because it utilizes a greater bit depth, 16 bits instead of 8, modifications to the camera-captured data can be reduced or altogether eliminated.

The raw format differs significantly from tiff and jpeg. The image data captured as 'raw' is not manipulated by the camera firmware, but is a proprietary format specific to the camera

manufacturer. As such, it is usually unreadable by most scientific image processing software. Like tiffs, most raw formats are 16 bit and use lossless compression. Unlike jpegs and tiffs, the data are not interpolated, and the raw formats store unmodified digital number values. White balance and other image modification information is stored in a header file and is applied by external software rather than being automatically incorporated into the actual values by the camera like a tiff or jpeg images. In addition, raw images maintain a much greater dynamic range. When comparing a 16 bit image to an 8 bit image, there are  $2^8$  or 256 (0-255) possible tonal values. In 16 bit there are  $2^{16}$  variations (65536) For example, in an 8 bit image, a pixel with a value of 0 is black; that same pixel in a 16 bit image could contain any one of 255 values. This data richness of the raw format is important for a number of reasons, but is especially important in over and under exposed images, where an area which in a 8 bit jpeg image would be either 255 or 0 can have a wide range of values in a 16 bit format allowing one to extract valuable data (Verhoeven, 2010).

As noted, each camera manufacturer has developed their own raw format, but each collects similar information. Raw files contain the digital numbers that represent the analog photon count from the sensor, and a header with all the metadata needed to convert the file into a jpeg, including exif data which contains camera and image metadata, white balance and exposure, as well as a thumbnail image. The sensor data without the metadata applied is visually unappealing. The only settings that affect the raw files digital numbers are ISO, shutter speed, and aperture.

When using a raw file it must be first saved as a raster image but only images without white balance, gamma correction, etc. can give accurate reflectance information. It is possible to export a raw file to a tiff and set the color interpretation to neutral so that the output represents the raw file's unmodified digital number. Dcraw is an open source program developed to do just this. With it, it is possible to export the pure digital numbers to a tiff for viewing and use in remote sensing software packages (Aber et al., 2010; Bennett & Wheeler, 2010; Curtin, 2007; Verhoeven, 2010).

## **2.4 Dcraw and ImageJ: Getting Images of Raw Digital Numbers**

To avoid the pitfalls of image interpolation, namely the modification of the original digital numbers from the sensor, one can use two free pieces of software, ImageJ and Dcraw, to extract unmodified sensor data. This workflow creates images with pixels representing raw digital numbers. Dcraw is a program that resulted from the need to decode proprietary raw image formats. Using it, one can not only specify precisely how the image is to be interpolated, but, more importantly, can also specify that the digital numbers be exported with no interpolation at all. The uninterpolated tiff, a black and white image with a 4x4 pixel array pattern (e.g. r,g1/g2,b representing the output from the camera's sensor) is not very useful, either as a visual tool or for calculations. The digital numbers for the separate channels cannot be compared because they inhabit adjacent pixels instead of overlapping. Using ImageJ, a free image manipulation program, one can obtain overlapping pixels without interpolation. In this case each channel's pixels are separated out into single color images rather than interpolated, so a pixel's position and size is altered rather than its value. This is accomplished using a publicly available macro in ImageJ which breaks the 4 pixel array apart (red, blue, green 1, green 2), expands the size of each pixel, and exports each of the 4 pixel types as a new tiff. The final product consists of 4 images with  $\frac{1}{4}$  the resolution of the original image. Each single color pixel is expanded to cover the neighboring other colors when the images are stacked.

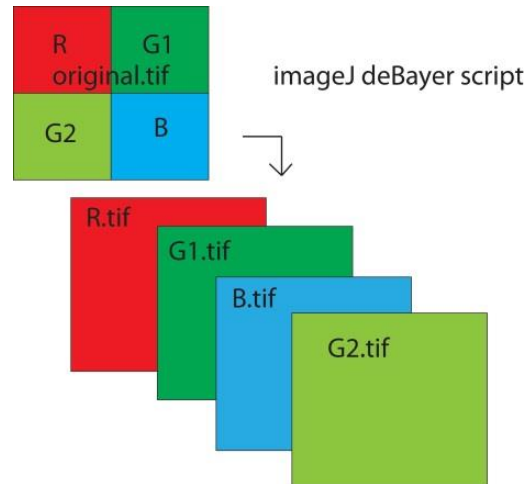


Figure 3. Uninterpolated raw pixels to image stack.

The figure 3 above shows the separation and stacking of one pixel of each channel which is what ImageJ accomplishes. This image stack can then be used for analysis like a traditional RGB image but with values that remain true to the original sensor digital numbers (Reyes, 2013; <http://imagej.nih.gov/ij/>).

## 2.5 Shutter Automation and Canon Hack Development Kit (CHKD)

One difficulty taking pictures with an UAV is how to remotely trigger the shutter. Three approaches exist to resolving the problem of taking pictures of an area of interest when the photographer cannot be there in person. The first is to remotely trigger the shutter on demand, the second is to automatically capture images at a specified interval whose frequency is rapid enough to guarantee coverage of the area of interest, and the third is to take video and extract the individual frames that capture the area of interest. Of these remote triggering is the most complicated but potentially offers the most efficient use of the camera. Using still frames from a captured video is the easiest method but provides the lowest quality images, likely below acceptable standards. The third method, taking images at a regular interval, captures unnecessary images that will need to be identified and culled from the dataset, increasing the time needed to prepare the image set for use. That said, much less time is needed for this activity than using video stills and the image quality will be much higher.

On-demand remote trigger shuttering may seem the best option-- providing the best coverage and image quality while reducing post-processing time. However, to record large areas a photographer would have to be aware of locations and frequently pressing a button to activate the shutter. In many instances, the better method is to take images at predetermined, programmed intervals. For large areas that need consistent photo coverage, images taken at timed intervals are a good option. Where images taken at specific locations are desired the only way to accomplish this is to have the shutter triggered not by the photographer or pilot but by a script that utilizes location taken from the UAV autopilot or GPS chip.

Which image capture method is to be used on a UAV also influences camera choice. The larger DSLRs often have the ability to use a remote control to activate the shutter wirelessly. These heavier, higher quality cameras often have functions that make them easier to use remotely and often can take very high quality video. These options would make a DSLR a good choice but their weight often disqualifies them from use in a UAS.

Choosing the remote trigger shutter method in a smaller, lighter camera severely limits choices. When using a search-by-feature function on <http://www.dpreview.com>, a comprehensive digital photography website, only 13 models of 838 combine a remote shutter feature (controlled via radio control from the ground), low weight (<500g), and manual focus. Adding a CCD sensor drops the camera choice to 3. But other options can expand camera choice without sacrificing function (<http://www.dpreview.com>).

A group has developed open source code, called Canon Hack Development Kit (CHDK). This code is legal, free, temporary, and does not void cameras' warranties. For Canon products, it allows much greater control of cameras' operations than the manufacturer initially provides. The code modifies the camera's firmware and gives the user control options often only available on DSLRs, and even some features not available on any standard, even DSLR, camera. These control features include increasing shutter speeds and ISO far beyond factory limits, and enabling use of the camera's autofocus beam as a motion sensor shutter trigger. The code also allows cheap point and shoots to record images in a raw format, greatly increasing their utility. All of these functions are activated by using scripts that are included in the code. Some of the most important functions for image capture in a camera mounted on a UAV which are not present in consumer cameras are a USB shutter trigger interface and an intervalometer, both of which can be

enabled with the CHDK code for a point and shoot Canon camera. An intervalometer automatically triggers the camera's shutter at pre-defined intervals (<http://chdk.wikia.com/wiki/CHDK>).

There are two main intervalometer scripts (i.e., shutter triggering protocols) to which the code provides access, with differences that are important for obtaining successful images in different conditions. The first intervalometer script is included in the initial package of default scripts initially downloaded with CHDK. The second is user-contributed and is called a 'fast intervalometer'. The default script has stated intervals of one second and greater. Image acquisition relies on the camera's automatic image settings, which can include autofocus, shutter speed, and auto-exposure. Each image will be shot as soon as each of these automatic settings are adjusted for the current image conditions. If the camera's shutter speed is manually set to a sufficiently fast speed to compensate for the motion of the UAV, the pictures will be appropriately focused and exposed no matter what the area of interest looks like or how it is lit. However, the disadvantage of this intervalometer setting is that the focusing and exposure process takes time, limiting the interval to 1 second or more.

The 'fast intervalometer' uses a camera's continuous shot mode. This script can order the camera to take images as fast as the camera can snap on its continuous shot setting. For example, the image acquisition rate of a Canon S95, the point and shoot camera we chose for our project, is 2-3 per second. This 200-300% increase in speed over the default intervalometer is due to the script relying on all image parameters being static. No time is spent changing settings based on changing environmental conditions. This means that if the settings are not manually pre-set, the first image taken by the camera will determine the focus, exposure, and other settings for all subsequent images. As a result, the tradeoff of greater image coverage is more time spent setting up the camera and less flexibility for changing conditions once the camera is aloft for variables such as elevation and lighting.

The fast intervalometer is better suited to times where the shooting conditions remain constant and greater coverage is needed. This includes flights at an elevation beyond the infinite focus range, a point beyond which a subject is far enough away that the maximum focus can be used. This value varies with camera models. For a Canon S95 the distance at which infinite focus can be used is anything beyond approximately 10m. If using the fast intervalometer, it is essential

for this camera to collect well focused images, so the flight must be planned so that the altitude above the highest object filmed is at least 10m. This planning must consider areas with high relief features, especially trees. The slow intervalometer is best used when the area contains target features under variable conditions that will require mid-flight exposure or focus changes to maintain image quality, and includes very low elevation flights where focus cannot be set to infinity and image sharpness is at a premium (Aber et al., 2010; Bosak, 2012).

## **Chapter 3: The Near Infrared**

### **3.1 Introduction: Beyond the Visible Spectrum**

An average human eye contains structures to discriminate between three bandwidths of the electromagnetic radiation spectrum. These wavelengths to which the eye is sensitive are called visible light and the three divisions are called colors. The eye's color-sensing structures are called cones. There are three types of cones, each sensitive to a certain bandwidth of light, with peaks at 420-440 nm (blue), 534-555 nm (green), and 564-580 nm (red). The human eye is sensitive, to some degree, to all wavelengths from about 380 – 720 nm, but becomes less sensitive to the light at the far ends of this spectrum. Consumer photographic equipment is designed to capture and display light in ways analogous to the patterns native to the human eye. Cameras thus divide and focus on capturing three broad bands of light in the red, green and blue wavelength ranges. Monitors and inks also use these three broad bands to display what the camera has captured (Curtin, 2007; Verhoeven, 2008).

For the purposes of the following discussion the difference between a channel and a band must be made clear. Bands are sections of the electromagnetic spectrum, of which visible light is a part. Channels are divisions into which the electronic image capture and display system is separated. For the vast majority of consumer cameras and monitors (designed to be analogous to the human eye) there are only 3 channels and they are called red, green, and blue but there can be any number of bands, depending on the width of the band. Each channel captures and displays a band. There are important scientific applications for bands that are made up of wavelengths beyond those the human eye can perceive. To view this data or record it using consumer cameras,

it must be captured and displayed using this channel substitution approach. This means that one or more visible bands must be removed to make room for the extra-visible band.

When attempting to display data in the NIR, one must substitute the red, green, or blue band for the NIR band. In satellite false color NIR imagery the traditional method of view the data is to display the NIR band in the Red channel, map the red band to the green channel, and the green band is mapped to the blue channel. The blue band is dropped (Sloan, 2013; Verhoeven, 2008).

### **3.2 Filters**

The purpose of the hotmirror is to primarily filter out wavelength bands beyond the visible spectrum on most consumer cameras. When it is removed, each channel records its original band (red, green, or blue) plus near infrared and ultraviolet bands in amounts that depend on the transmissivity of the pigments used in the Bayer filter. To get useful data from the camera for research purposes for bands beyond the visible spectrum, some of these visible spectrum bands must be filtered out, by employing one of a variety of other filters. Often the filter manufacturer will provide a spectral response graph, showing the light that is blocked and passed by the filter.

If a filter passes all wavelengths greater than a certain length it is called a longpass filter. If it blocks all wavelengths shorter than a certain length, it is called a shortpass filter. If it passes just a certain wavelength it is called a bandpass filter and if it does the opposite, blocking a certain wavelength, it is called a notch filter (Table 3). A hotmirror is a bandpass filter, passing

just visible light. The Hoya red 25A filter used by Rabatel et al. (2011) whose transmission curves can be seen in figure 4, is a longpass filter, passing all wavelengths red and longer.

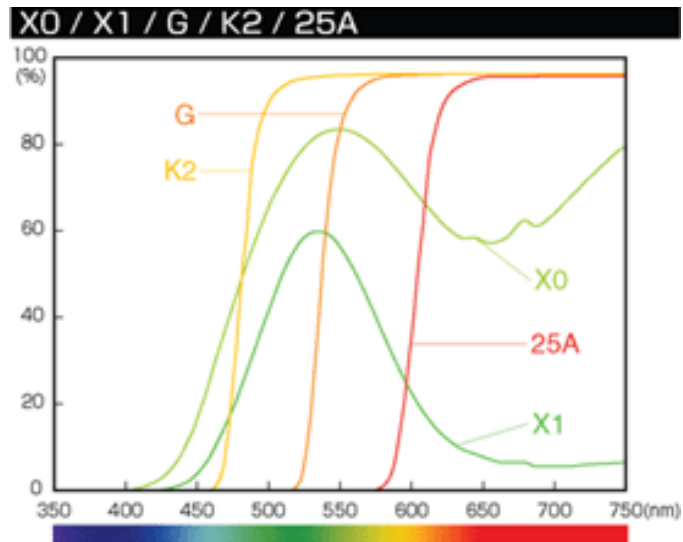


Figure 4. Hoya's filter transmission curves. (<http://www.hoyafilter.com/hoya/products/coloredfilters/25ared>)

A shortpass filter, for example, might be used if one wanted to isolate the ultraviolet capabilities of a digital camera, blocking blue wavelengths and longer (Verhoeven, 2008; <http://www.maxmax.com>; <http://www.edmundoptics.com/>).

filter name	filter function	Filter example
longpass/highpass	filters light shorter than a certain wavelength	Hoya red 25a: filters all wavelengths < 600 nm
shortpass/lowpass	filters light longer than a certain wavelength	Maxmax xnite330c: filters all wavelengths > approx. 400
bandpass	filters all but a specific band of light	hotmirror: passes only light between approximately 400 -700nm
notch/bandstop	filters only a specific band of light	Edmunds Rugate 632: filters from approx. 620nm - 640nm

Table 3. Filter Types

### **3.3 Near Infrared (NIR)**

Near infrared images can reveal plant stress. The source of the stress can be any number of things including insect infestation, poor soil chemistry, or, most important to this study, a lack of water. The camera we chose to mount on the UAV for the project is capable of recording imagery in the near infrared (NIR) spectrum. NIR spans wavelengths from approximately 750 nanometers to 1400nm. There are specialized sensors employed in professional multispectral cameras that can record NIR wavelengths. These specialized cameras are designed to have little to no overlap between bands. The ability to discriminate clearly between bands is part of what gives these systems high spectral resolution. Consumer camera bands often overlap each other. Without considerable post-processing work or complex filters, when NIR and UV light are added, the spectral resolution of these cameras drops considerably. This is the reason that a high spectral resolution professional multispectral camera is desired for NIR and UV work. However, the cost of multispectral cameras, especially those light enough for use on a UAV, are too expensive to consider for the modest budget research project, and the image resolution of these cameras is frequently very poor.

Lightweight inexpensive, consumer grade camera have sensors that offer better resolution and are also sensitive to wavelengths outside of those visible to the human eye including NIR and UV wavelengths. However, manufacturers use hotmirrors to reduce the recording of NIR and UV wavelengths, because including these spectra in images gives them an unnatural appearance. One can remove this filter and replace it with another to select for specific wavelengths (Rabatel et al., 2012). Figure 5 illustrates the process by which NIR and visible light can be captured simultaneously by a single digital camera.

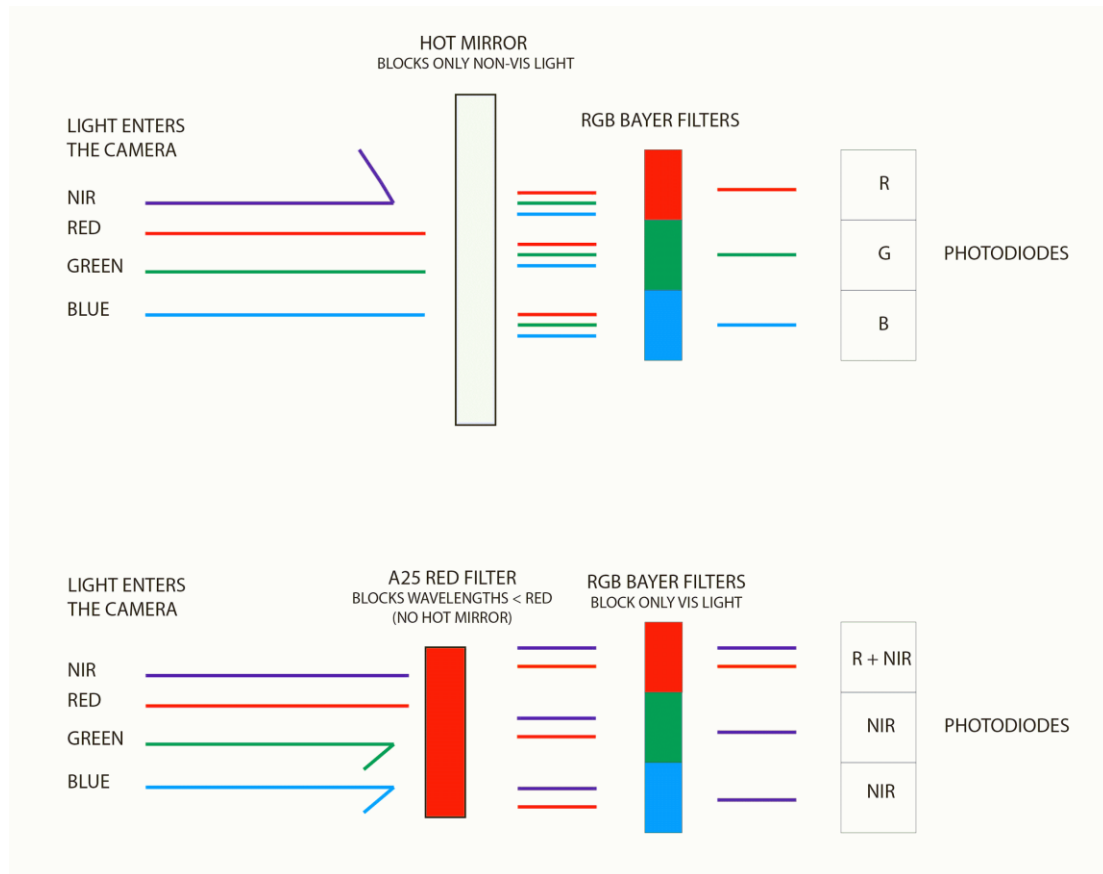


Figure 5. Behavior of light entering a standard camera and a camera with the hot mirror replaced with a red filter

There is rising interest in UAV-based multispectral imagery for scientific research. However, the existing cameras manufactured specifically for this purpose are both expensive and feature poor when compared to even consumer-grade cameras. The least expensive version of Tetracam's ADC multispectral cameras, standards in the industry, sells for more than \$4000, but has an image resolution of only 3.2 megapixels, and a maximum image capture frequency of 1 every 3 seconds (<http://www.tetracam.com>).

Any silicon based camera sensor can record NIR wavelengths, and can detect wavelengths up to about 1100nm (Verhoeven, 2008). Relatively simple procedures convert consumer digital cameras to record NIR. A converted consumer camera also retains all of its other functionality, including image resolution, that is absent in specialty NIR cameras. For example, the Canon s95 camera used in this research, converted to record IR by Maxmax

([www.maxmax.com](http://www.maxmax.com)), a company that performs camera modifications including hotmirror removal, has 3 times the resolution, captures images 3 times faster, and is less than a quarter of the price of Tetracam's multispectral camera. However, while using a converted consumer digital camera to capture only infrared light is easy and capturing both infrared and visible light combined in a single channel is easy, using a consumer camera to capture both infrared and visible light simultaneously *without mixing the two* is extremely complicated. Most commonly, multiple cameras, multiple sensors, or multiple shots of the same scene are required. These methods are fraught with difficulties. Most multiple shot and multi-camera methods necessitate image rectification in the post-processing step to account for changes in camera location or scene change. Additionally, for systems mounted on a UAV, the weight of multiple camera systems is prohibitive. Moreover, taking pictures from precisely the same location is logistically nearly impossible (Lu et al., 2009).

### 3.4 Vegetation Indices

The Normalized Difference Vegetation Index is a useful calculation that compares channels to assist in the analysis of landcover using multispectral imagery. The NDVI is calculated by normalizing the difference between a visible band and the NIR band.

$$\frac{(NIR - VIS)}{(NIR + VIS)}$$

A plant that is stressed will appear dull in NIR images. Healthy plants, on the other hand, will be bright. However, because materials besides vegetation reflect NIR, the Normalized Difference Vegetation Index (NDVI) was developed to provide a method of narrowing down the spectral response to vegetation. Red light responds the opposite way to vegetation as NIR. Healthy plants absorb it and unhealthy plants reflect it. Normalizing the NIR with red better captures vegetation health. The NDVI and NIR can be used to identify a plant species' unique spectral response or to determine areas of varying vegetation stress levels, possibly indicating differing access to moisture.

There are many other indices that return information relevant to the status of vegetation but most of them require much higher spectral resolution than the NDVI (Dworak et al., 2013; Ashraf et al., 2011). To calculate a simple vegetation index like the NDVI one needs two bands, one of visible light and one of infrared light. In an ideal scenario (using a camera with no hotmirror and a red filter) in addition to visible red light the camera's red channel would capture the same values for IR as the blue channel. The captured image can be thought of as one clean IR band in the blue channel and one 'dirty' visible + NIR band in the red channel. Because the red channel is simply the sum of red light and NIR light, one could 'clean' it by subtracting the NIR values captured in the blue channel (Rabatel et al., 2011).

$$\text{clean NIR band} = \text{blue channel}$$

$$\text{clean visible red band} = \text{red channel} - \text{blue channel}$$

The problem with this method is the assumption that the NIR captured in the red channel is equal to the NIR captured in the blue channel. This is not the case. The amount of NIR captured in any one channel depends on the pigment used in the Bayer filter and the NIR wavelength (Verhoeven, 2008). The amount of NIR captured in each channel varies greatly. Predicting the amount of NIR light recorded in a visible channel is extremely difficult, depending on the filters, sensor, and subject. Thus, obtaining a visible light band with no influence from NIR is the main obstacle to using a single camera to capture both visible and NIR light.

Remote sensing often employs various band ratios and calculations, called indices, to extract more information from an image than is readily seen with the naked eye. When using multi or hyperspectral sensors, the available bands can be very precise, sometimes just a few nanometers wide, and there are often a choice from a wide variety of bands to use. For example, satellites like the Earth Observing 1 carry a sensor capable of recording and discriminating among over 200 different bands (<http://eo1.usgs.gov/>). Using a consumer digital camera limits the number of available bands for use in indices. Because a consumer camera has only three channels whose bandwidths are quite wide, indices should be limited to those that use no more than three wide bands to facilitate the mapping of the bands to the camera's 3 channels.

Using a consumer camera from a low altitude versus higher elevations helps to resolve some of the difficulties in determining vegetation indices with a limited number of bands. Chlorophyll has a very similar spectral response to red and blue. This means that if blue light is

available, it may be used in the place of red in indices. When using images taken from a low altitude there is little Rayleigh scattering of the shorter wavelengths, so there should be few concerns about radiometric errors caused by using the blue band from high altitudes (Knoth et al., 2013). This makes a blue NDVI possible. One concern that is not addressed in the literature is the different response of a blue-NDVI to different landcover types.

Other indices available are listed in Table 4.

Red-NDVI	$(\text{NIR}-\text{RED})/(\text{NIR}+\text{RED})$
Blue -NDVI	$(\text{NIR}-\text{BLUE})/(\text{NIR}+\text{BLUE})$
Green - NDVI	$(\text{NIR}-\text{GREEN})/(\text{NIR}+\text{GREEN})$
ENDVI <sup>2</sup>	$((\text{NIR}+\text{GREEN})-(2*\text{BLUE}))/((\text{NIR} +\text{GREEN}) + (2*\text{BLUE}))$
greenness index	$\text{GREEN}/(\text{RED}+\text{GREEN}+\text{BLUE})$

Table 4. Consumer Camera Vegetation Indices

### 3.5 Single Camera Visible/NIR Photography Methods

Currently, some of the best work to capture a ‘clean’ visible and NIR channel with a single camera has been done has been by Rabatel et al. (2011, 2012). They outline a method to determine the relationship between the IR sensitivities of the 3 different channels and develop an equation to create two virtual channels that match preselected wavelengths (Rabatel et al., 2011). Unlike some, Rabatel uses all three channels, finding a combination that best mimics the desired virtual channels. To accomplish this, work was done to calibrate their camera, a Canon 500D. The calibration consisted of testing the spectral response of the channels to 10 nm wide bands of light from 440nm to 990nm using the monochromator from a spectrophotometer. The average value from each 10nm band image for each channel when graphed shows the sensor’s spectral

<sup>2</sup> developed by Maxmax (<http://www.maxmax.com/endvi.htm>)<sup>2</sup>

response curve. Rabatel's method is precisely calculated for an individual sensor and can only be used once the sensitivity curves are known (Rabatel et al., 2011). The authors chose a Wratten Kodak no 25 filter to produce a red and an NIR band with mid-height bandwidths of 600-670 nm and 760-830 nm (Rabatel et al., 2011). In their subsequent paper, Rabatel et al. (2012) present the following equation to derive their virtual bands when using the Hama Rot R8 (25 A) longpass filter with a 600nm threshold:

$$P(r(\lambda)) = 0.0968 * c1(\lambda) - 0.1722 * c2(\lambda) + 0.0842 * c3(\lambda)$$

$$P(nir(\lambda)) = -0.0455 * c1(\lambda) + 0.0010 * c2(\lambda) + 0.2605 * c3(\lambda)$$

Where  $r(\lambda)$  /  $nir(\lambda)$  = desired red / near infrared sensitivities and  $c1, c2, c3$  = camera channels

They note that this equation works for multiple, similar camera models but do not mention how they verified this nor do they comment on how widely their equation might be used on different cameras (Rabatel et al., 2012). This is problematic because unlike computer processors that are shared across several models, camera sensors are rarely common among different camera models even in the same brand. Occasionally upgrades to lenses or camera software become a new camera model without a sensor upgrade but usually new models contain new sensors (<http://www.dpreview.com>). Because nearly every sensor and Bayer filter combination is unique, each camera should have its spectral sensitivity mapped (Verhoeven, 2008).

Some researchers have opted to use the blue channel as the visible band and the red channel for NIR using a filter to block red light instead of blue, stating that "NIR radiation (up to about 830 nm) is mainly recorded in the 'red'-band" (<http://www.maxmax.com>). Though this approach has been used with some frequency, most notably in the open source work found at [publiclab.org](http://publiclab.org) and the plant stress camera offered by [maxmax.com](http://www.maxmax.com), there has been little work presented to address subtraction of the NIR influence in the visible channel (<http://www.publiclab.org>; <http://www.maxmax.com>).

This NIR influence is the result of the difference in sensitivity to NIR of each channel. Based on published spectral responses a camera's blue channel records NIR light just as the red channel does but in differing amounts at different wavelengths depending on the pigment used in

the Bayer filter. Without separating out the blue channel's NIR and visible light response as Rabatel et al. (2011, 2012) did with the red channel, it is very likely that results of the blue-NDVI are inaccurate as the visible channel will be mixed with NIR. For some camera models this will be especially problematic at the NIR wavelengths above ~850nm where many sensors' blue channel is more sensitive to NIR (see spectral response graphs). Knoth et al (2013) do mention that they had difficulty with this but that because the majority of the NIR < 850nm was recorded in the red channel and longer wavelength NIR was evenly distributed the use of a mixed visible/NIR channel seemed reasonable and recommended the use of the much more expensive Tetracam products if a more spectrally accurate product is needed (Knoth et al., 2013). Among the groups currently using a mixed NIR/visible channel in an NDVI for UAV based remote sensing is the USGS. They published a document giving instructions on how to compute a red-NDVI without correcting the mixed NIR/visible channels (Sloan, 2013).

Other methods have been proposed to solve the problem of NIR/visible capture with one camera, but none have been easy to implement or obviously successful. These methods include a change to the Bayer filter and the use of new demosaicing algorithms (Lu et al., 2009) and using multiple sensors and a prism rather than a Bayer filter to separate out channels (Biasio et al., 2010). At first glance the work of Lu et al. (2009) seems promising, but the authors ask the reader to assume that all Bayer filters transmit IR light equally. As the unequal transmission of IR is the primary obstacle to resolving this problem, this method is unlikely to be successful. Biasio et al. (2010) were very successful. Their setup captured three visible channels and two NIR channels by using multiple sensors within one camera with no image rectification problems. The solution is straightforward, but the equipment is expensive and heavy. Both of these characteristics eliminate this approach in a cost-conscious UAV program. Dworak et al (2013), understanding that adjusting for each channel's unique response to NIR wavelengths might not be necessary, selected a sensor with a relatively uniform response to NIR for their research. They successfully automated the discrimination between soil and vegetation, calculating an NDVI using a sensor where the red and blue channels responded the same to wavelengths at 830 nm.

An analysis of many sensors reveals that this is equal response at the higher end of the NIR band is not uncommon. Eight out of nine spectral response curves show that the blue and red channels respond similarly to wavelengths at approximately 850 nm. Unfortunately, at 850 nm

the sensor sensitivity is much lower than at shorter wavelengths so the images will have to be treated as if they are being taken at low light. This equal response means that basic math could be used to create an NDVI. Although the total response is much lower than at shorter wavelengths, the NDVI's normalizing should make this disparity a non-issue as long as the image is of sufficient quality.

To take advantage of this band of equal response, a notch filter should be used in combination with a longpass filter, blocking wavelengths shorter than green and blocking NIR light from about 700 nm to 850 nm. Landsat 8's OLI sensor's NIR band uses NIR wavelengths from 850nm-880nm, so using wavelengths longer than 850nm fulfills another important role. By using these longer NIR wavelengths one can create new datasets that can be compared to existing Landsat datasets, a standard remote sensing product with a long continuous history of collection. Because older generation of Landsat used broader NIR bands (TM and ETM bands use from 760/770nm to 900nm), matching the older Landsat datasets will be very difficult.

### **3.6 Spectral Response Curve Examples:**

The manufacturers of cameras intended for research publish the spectral response curves for their products. Additionally, some who are using or producing modified consumer digital cameras to capture near infrared images have recorded the spectral response curve of their cameras' sensors. Figure 6 displays 6 of these spectral response curves for different consumer grade cameras. The lines correspond to the camera's red or blue channels' sensitivity to light at certain wavelengths with the hotmirror removed. The graphs display the wide variety of response per camera model. The response can be used to pick a filter and NIR image processing technique. For instance, as long as the red and blue channel response to NIR is the same, a basic subtraction approach can be taken to removing NIR from the visible light channel. For the Nikon models, the graphs suggest an approach that focuses on either NIR light above 850nm or NIR wavelengths between 700-750 NM. At 850nm, basic subtraction could be used, whereas at 700-750 the blue channel response to NIR is so limited its influence might be acceptable when computing NDVI. Both of these proposed solutions would require a complex filter. The 700-750nm approach would use the blue channel for visible light and the red channel for NIR. This requires a double notch filter allowing

only blue visible and NIR between 700-750 nm to enter the camera. The  $> 850\text{nm}$  approach would require a double notch filter that allows only red visible and NIR above 850nm.

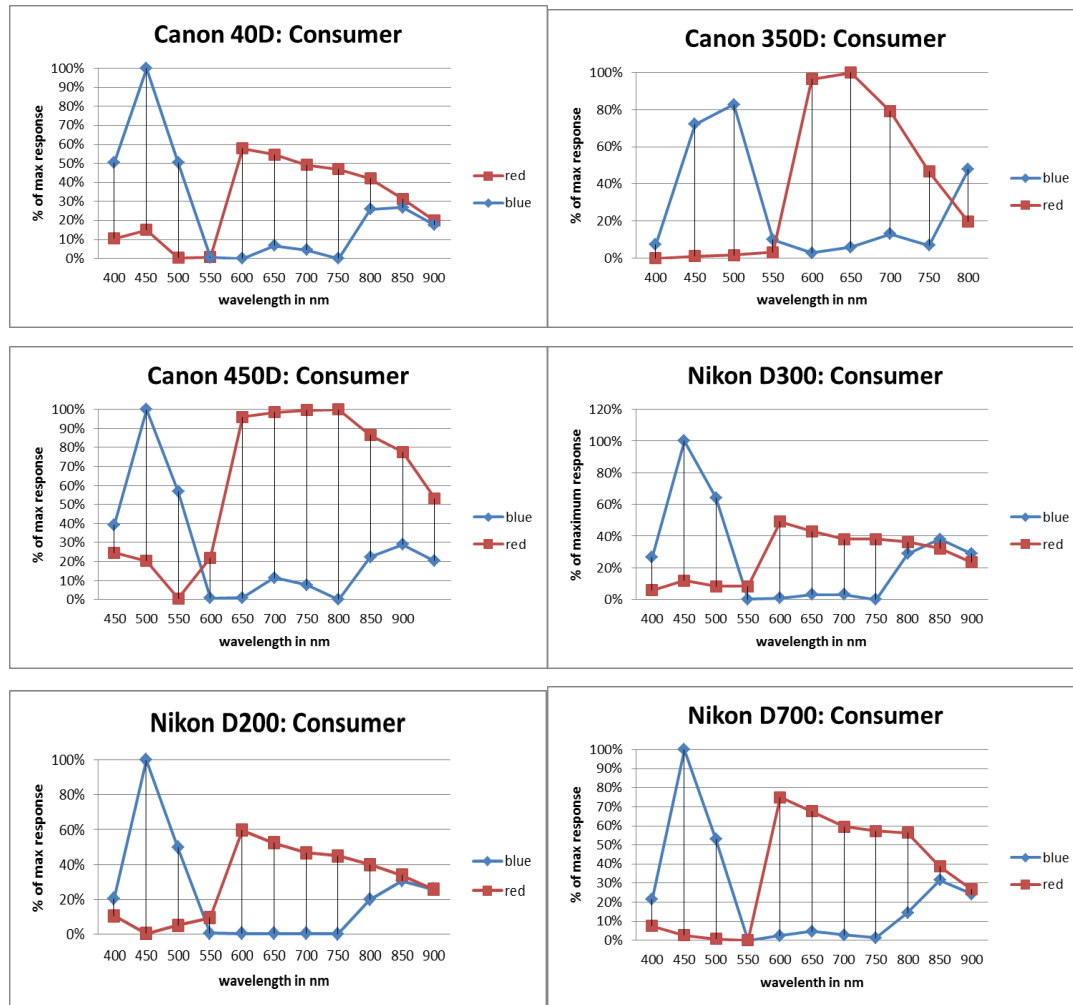


Figure 6. Spectral response curves of 6 consumer cameras.

### 3.7 Selected Camera:

For our project we used a matched pair of Canon S95 high-end point and shoot cameras; one in the original state of the manufacturer, one modified by Maxmax to remove its hotmirror. Currently there is no spectral response graph available for this camera model. This 10 megapixel, 195g camera uses a 1/1.7" CCD sensor which fits in the large sensor point and shoot category. It provided high resolution images with relatively low distortion when in motion. It has a manual

mode for focus, all exposure factors (ISO, shutter speed, and aperture), white balance, and it can be controlled by CHDK. Its maximum shutter speed is 1/1600 of a second and it has a maximum capture rate of 3 images per second. A Hoya A25 high-pass red filter with a cut off of 600nm was chosen to emulate Rabatel's methods of recording NIR imagery (Rabatel et al, 2011; <http://www.hoyafilter.com/hoya/products/coloredfilters/25ared>). The camera choice was driven by meeting the criteria of CHDK compatibility, sensor size and type, low weight, manual settings, and modified by Maxmax. Having a matched camera pair also ensured camera accessory compatibility (batteries, memory cards, CHDK versions) and a reduced learning curve.

## **Chapter 4: Structure from Motion (SfM)**

### **4.1 Introduction**

Our research project used a relatively new method, called Structure from Motion (SfM), to produce 3D surface models rather than the traditional stereo-pair photogrammetry. SfM is a fast, economical way to produce 3D surface models from an unstructured /unordered series of images. One of the major drawbacks of SfM is that it does not work well on vegetation, for multiple reasons. SfM is designed to work on rigid objects. Due to wind, vegetation, especially tree canopy and grasses, is rarely rigid. The three-dimensional complexity of particularly woody vegetation also creates challenges for three-dimensional modeling.

SfM was developed in the field of computer vision. The original software was developed to create 3D models from images collected from the internet for virtual tourism (Snavely, 2007; Snavely et al., 2008). SfM photogrammetry does not need camera parameters or location information to be known with high precision a-priori which requires expensive, medium or large format metric cameras in traditional photogrammetry. Instead SfM matches a very large number of images simultaneously and in the process derives the camera parameters. For this reason the cameras do not need to be calibrated, and any combination of multiple camera settings including focal lengths can be used. In fact, multiple, different model cameras can be used. Because the process uses so many pictures (the more the better) lower quality, consumer grade cameras can be used. One weakness of SfM's reliance on a high number of overlapping images is that borders of project areas are prone to error due to a reduction in overlap. In addition to the much lower

equipment cost there are many open source software packages that reduce the cost of SfM. Many of these packages were used by the authors referenced in this paper. This means that the entire SfM process can be performed for the price of a computer, a common digital camera, and processing time (It should be noted that Photoscan, the SfM program used in this research is not open-source, but there are lower-performance open-source programs available.) (Westoby et al. 2012).

While SfM is computationally intensive, it does not require a high level of expertise. The majority of the process is entirely automated. SfM creates a point cloud in relative coordinates, which must be translated to real-world coordinates by performing a linear transformation based on ground control points (GCPs), which must then be then interpolated to create a digital surface model (DSM). Consequently, the elevation data can only be as accurate as the GCPs. This requires highly accurate GPS receivers and enough time to establish a sufficient number of GCPs that can be seen in the photos and are distributed across the study area. An even distribution will prevent skewing the data during the translation. A secondary result of this is that the biggest investment of money and person hours is usually the establishment of GCPs (Westoby et al. 2012).

At the heart of the SfM process is the transformation of 2 dimensional pixels (picture elements) into 3 dimensional voxels (volume elements or volumetric pixels). To do this, an SfM program finds features common to several images. It then uses the equivalent of human stereo vision from more than two images to determine the location of each target feature relative to all the other matched features, and assigns it coordinates. If there are unwanted features in an image, e.g. reflective surfaces, moving objects, or vegetation, one can create a secondary mask image to prevent the software from trying to find matches for these features. The unwanted features in the primary image are then skipped when the overlying mask image indicates that they are to be ignored (<http://www.agisoft.ru>).

## **4.2 SfM Versus LiDAR**

Any discussion of SfM must include comparisons to Light Detection and Ranging (LiDAR). A LiDAR system emits thousands to hundreds of thousands of laser pulses per second. The time between when each pulse was emitted and when it is reflected back to the system is

used to determine the distance the pulse traveled. Because the location of the emitter, the pulse's direction of travel, and the distance the pulse traveled are all known, the location of the object from which the pulse was reflected is also known. The pulse from the LiDAR system is not a dimensionless point but has a footprint whose dimensions are determined by the system and the distance of the system to the reflecting surface. When a pulse is only partially intersected by an object the rest of the pulse continues on to reflect off of surfaces farther from the system. In this way a single pulse can have multiple returns that represent different objects. The location of every object hit by all of these pulses is known, and the product of a LiDAR scan is a cloud of points that represents a 3D model of the scanned surface. This scenario often happens at the edges of buildings or leaves. Based on these returns one can, for example, determine canopy density by counting total number of returns, classify buildings versus ground based on finding building edges with 2 returns, and find tree heights by subtracting last return from first returns. One can also create a DSM by using only first returns or create a bare-earth digital elevation model (DEM) by using only points classified as 'ground' (Akay et al., 2009).

LiDAR is a highly accurate method to produce 3D images of landcover features; and it 'sees through' vegetation using multiple returns but is not superior to SfM in several respects. LiDAR surveys are conducted both terrestrially and aerially. Research has shown that low altitude SfM products can produce a point cloud far denser and more accurate than that produced by the first returns of an aerial LiDAR scan when the features being recorded have little vegetation and are of heterogeneous texture. However, SfM point clouds are inferior to the density and accuracy of a terrestrial LiDAR scan and cannot match the information that accompanies both aerial and terrestrial LiDAR's multiple returns in vegetated areas (James & Robson, 2012). In most circumstances, if one has the resources, one should opt for LiDAR. On the other hand, for those on a limited budget, the cost of LiDAR is impractical. LiDAR equipment is heavy and expensive. SfM technology is cheap and light, and the data obtained from a low altitude SfM flight, if collected and processed correctly, will better the first returns of an aerial LiDAR survey. SfM also includes point data in color-- in addition to location. Furthermore, SfM allows matching individual pixels to points, which enables remote sensing image classification to be used. This creates a detailed and customizable point classification system than that offered by LiDAR. In our research, we concluded that in some circumstances LiDAR is the

only valid option; in others, including for our research project, SfM is more than satisfactory, is inexpensive, and offers some features that improve on LiDAR results.

### **4.3 Accuracy**

Several studies have been performed comparing the accuracy of SfM to LiDAR in many environments: geologic and glacial landforms (Westoby et al., 2012); stream reaches (Fonstad et al., 2013); a small volcanic rock, a volcanic crater, and a sea-side cliff (James and Robinson, 2012); and a stabilized aeolian dune environment (Hugenholtz et al., 2013). All the studies demonstrate that SfM derived DEMs compare favorably with LiDAR data. James and Robinson (2012) found this to be true at multiple scales, from centimeters to kilometers. It was also shown that SfM results in denser point clouds (James and Robinson, 2012; Hugenholtz et al., 2013). Accuracy was found to be negatively affected by vegetation and homogeneity of surface textures (Hugenholtz et al., 2013; James and Robinson, 2012). Surprisingly areas of high relief and, in most cases, using static camera parameters were not shown to negatively affect the accuracy of the DEM (James and Robinson, 2012). Other factors beyond accuracy were also assessed. It was found that the time to process the data is much longer but much less manual using SfM rather than LiDAR (James and Robinson, 2012). Additionally, when using SfM the time for data collection is much less but the time preparing for collection is longer (James and Robinson, 2012; Westoby et al., 2012).

## **Chapter 5: Meadows**

### **5.1 Introduction**

The montane meadows of the Sierra Nevada are of critical ecological and hydrological importance. Meadows are the most biologically diverse of all Sierra habitats, perform invaluable water filtration and flow regulation, and can serve as an indicator of climate change (Debinski et al., 2000). Stream channels are the heart of functioning meadows. Stream channels replenish, and are replenished by, the water table, the driving force behind this ecosystem. Meadows filter sediment and store water. Streamflows emanating from meadows supply the Central Valley and San Francisco Bay Area with drinking water. Meadows help to ensure the quality and availability

of water as well as providing flood control. Because of these critical functions, it is imperative that montane meadow streams are well understood (Allen-Diaz, 1991; Olsen, 2009; Slocombe, 2014).

Montane meadows and streams exist at many scales. Meadows with small streams are underrepresented in the literature, but are as important to understand as their larger, better studied siblings. To understand meadows, the associated streams must be surveyed but small discontinuous stream channels, like those found in smaller meadows have been largely ignored. One exception to this is the work of Slocombe, who performed stream channel research in the meadows of the Sierra Nevada with small, healthy or recently restored streams. However, because ambiguous and obscured channels are defining features of these small meadows streams, terrestrial surveys of these meadows has been somewhat ineffective; the results largely subjective rather than objective and quantitative (Slocombe, 2014).

Small montane meadow channels are unique; they are formed of a series of scour pools connected by sod that acts as riffles or steps, rather than coursing over a gravel bed as is common with larger streams. These small streams undergo a wet/dry cycle that changes from overland flow to subsurface flow, depending on the season. Channels are very shallow and often obscured by vegetation, especially in the summer months when vegetation is full grown. Slocombe had great difficulty identifying stream channel location and morphology e.g. width and bankfull depth, due to the obscured channels and vegetated riffles. Slocombe found that sometimes channel boundaries may be detected based on vegetation change or topographic breaks but this is an inconsistent method (Slocombe, 2014).

The goal of our research project was to use remote sensing to improve on Slocombe's methods to describe and measure the principal features of these meadows. These features include channel width, bankfull depth, sinuosity, and straight reaches. We hoped to produce better results more quickly and less expensively than ground survey. Our hypothesis was that using remote sensing from a UAV aerial platform would identify a greater amount of the channel in a much shorter time than ground survey. The remote sensing methods we evaluated included LiDAR, photogrammetry, SfM, conventional 2D photography and NIR photography. Of these methods, LiDAR and traditional photogrammetry were impractical due to the price of LiDAR surveys of sufficient point density and, for photogrammetry, vegetation obscuring the stream channels. SfM

can be used, but would likely not be effective in providing accurate 3D information, again because of obscuring vegetation. Conventional photographs are able to show stream channels when the meadow is saturated with melt water, but it would be difficult to identify the main channels or morphologic features in these photographs. Finally, we hypothesized that using NIR would allow us to identify the main stream channels, especially when images are taken during the summer when water stress is predicted to be higher.

The practicality of using NIR for our research was based on literature that presented methods to identify stream channels using NIR imagery and what meadow and stream conditions might affect these methods. Blumberg et al., (2004) demonstrated that NIR satellite imagery can be used to identify stream channels when the channels were deeply buried or cut into the bedrock. While the scale of this project was larger compared to our project, in many ways the methods of the two studies mirror each other. Both sought to identify obscured stream channels and in both the presence of below-ground moisture created a unique spectral signature along the hidden channel. Further evidence of the utility of NIR for obscured channel identification was presented serendipitously in Loheide et al. (2009). Identifying meadow stream channels was not their stated purpose, but in the course of their research Loheide et al. acquired NIR imagery of montane meadows for vegetation analysis. It is evident from Figure 7 that the false color NIR imagery can be used to identify meadow stream channels. Again, the scale of Loheide's streams is much larger than those we studied but the image demonstrates a proof of the concept.

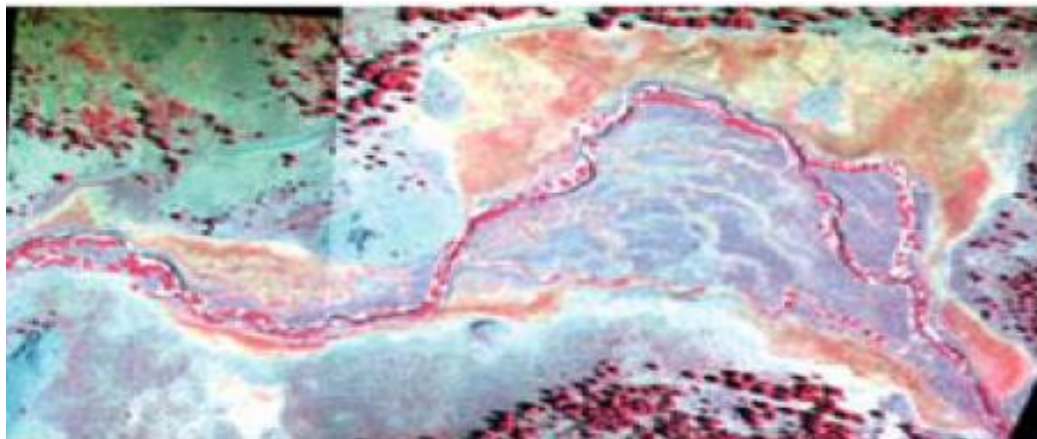


Figure 7. NIR imagery of montane meadows (Loheide et al., 2009)

It was hypothesized that vegetation type could be a valuable feature in stream channel identification. Using SPOT imagery which has multispectral bands similar to those of a converted consumer camera Peterson et al. (2001) were able to correctly classify two species of sedge (*Carex*) at 90.48% absence/66.67% presence. Sedges are a major component of the vegetation in the montane meadow stream channels and this study proved that it is possible to differentiate between plant species which when added to water stress could assist in channel identification. Once again, the scale of the research and the spatial resolution of the imagery used were far too large and coarse to make a direct inference about the success of similar methods in montane meadows. However, the study does prove that by using spectral bands capable of collection by an altered digital camera one can differentiate between common meadow species.

The hypothesis that a stream channel can be identified using NIR imagery is based on preferential access to water by in-channel vegetation versus vegetation outside of the channel. Several factors determine a meadow's water table level. When the hydraulic conductivity is low and lateral flow is high, the water table parallels the slope of the surface from the meadow edge to the stream channel. When hydraulic conductivity is high and basal flow dominates, the water table parallels the bedrock at the level of the stream channel. The use of NIR to identify small stream channels was predicted to be best in the case of basal flow because the channels would then be the closest to the water table. Fortunately, under most circumstances, the water table gradient is quite small in montane meadows, meaning that topographic variations are mostly responsible for varied moisture depths (Loheide et al., 2009).

Soil grain size also affects soil moisture depth. This determines which plants will begin to exhibit stress and at what point. Silts and loams support greater vertical capillary movement of soil moisture from the water table to the root zone. If the soil in a montane meadow is fine grained it will increase the likelihood of uniform plant stress by increasing the available moisture beyond the channel (Loheide et al., 2009).

Unlike the spring when meadows are inundated, a meadow's water table is predicted to be low enough during the summer to stress vegetation differently based on its location within or without the channel (Darrouzet-Nardi's et al., 2006). Evening water table levels are predicted to be lower than morning levels, possibly accentuating plant stress. It could be possible to fine tune the spectral response by time of acquisition. If evening acquisition resulted in uniform stress,

morning acquisition may have helped to differentiate vegetation types by allowing the channel vegetation to preferentially access moisture (Allen-Diaz, 1991, Cheng et al., 2013).

## **5.2 Problems with Stream Identification: SfM and NIR approaches**

Two approaches were used to study stream channels. The first used SfM to create a DEM of the meadow to determine stream channel location and depth. The second used NIR imagery. For SfM, the proposed meadows have conditions that were predicted to preclude usable results, viz. the channels are very shallow and have obscuring vegetative cover. Because the channels are shallow - in the 5 to 20 cm range - the resolution of the DEM would have to be exceptionally fine, finer than is possible using the planned technology when hindered by vegetation.

### **5.2.1 Results of SfM DEM Generation Using GoPro**

A proof-of-concept mission was flown in April of 2013 over our study meadow using a GoPro Hero 3 camera to capture still images. The GoPro camera was chosen because it is very small, extremely robust and waterproof: a perfect camera for test flights over a flooded meadow. The camera also has a fisheye lens. Ultimately, the physical advantages of weight and durability were outweighed by the difficulties in using photogrammetric software with a fisheye lens. The distortions of the lens resulted in distorted mosaics and 3D models (Figure 8). In an attempt to mitigate the issue, a mask was applied to all the images, limiting the SfM software to operating only on the center of the images where the distortion is less. This improved the result but the distortion was still noticeable. It should be noted that future releases of Photoscan include improved algorithms to make use of fisheye lenses. Future research may benefit from reprocessing the GoPro photos.

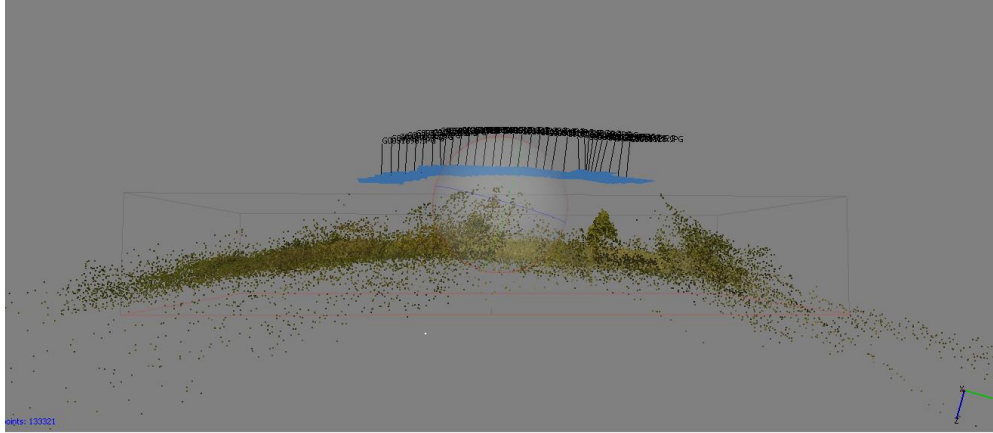


Figure 8. Warped ground plane created from GoPro imagery.

Our second approach was to detect and planimetrically map channels during the dry season using the NDVI or a similar vegetation index to identify hydric plants like many sedges (*Carex*). We predicted that the vegetation in and near the channel would be healthier than the surrounding vegetation because of greater available moisture in the channel. This difference in vegetation health should be visible in the near infrared (NIR) spectrum.

### 5.3 Meadow Methods and Results:

Two flights were flown above montane meadows north of Lake Tahoe in California, both at elevations of approximately 1500 meters. The first, Knuthson Meadow, has been restored using a pond-and-plug method, forcing surface flows into less incised historic channels. The meadow is vegetated with mesic to hydric vegetation as well as some willow and pine. At the time of the survey there was no surface water.

The second study area was a montane meadow called Dry Creek (Figure 9). The stream channel was incised less than 2 meters, with hydric vegetation growing within it. No water was present in the channel. Outside of the channel, the meadow was populated primarily with xeric vegetation such as sagebrush (*Artemisia*) and occasional pines, as is typical of an incised meadow. Very few scour pools were found along the reach and we found only one instance of an exposed gravel bed.

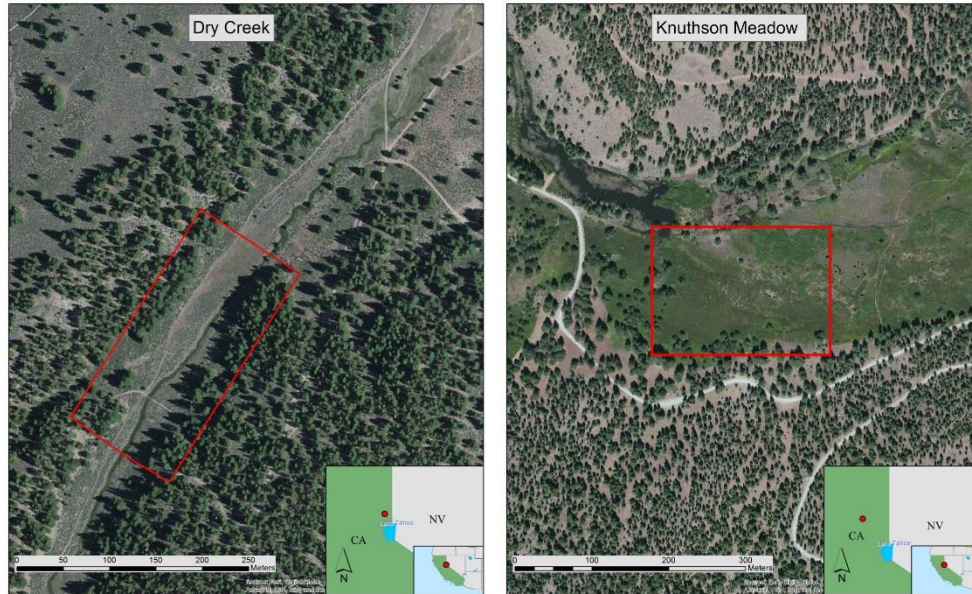


*Figure 9. Dry Creek (left) and Knuthson Meadow (right) Area Maps*

The flights took place near noon under direct sunlight at an altitude of 35 meters. Shadows were pronounced. The takeoff and landing were amid sage and other wood shrubs. Take off and flight were automated, but landing required manual piloting. The narrow meadow of Dry Creek resulted in poor GPS reception at ground level near the tree line requiring the takeoff to be moved to allow for successful autopiloting. The loss of propeller efficiency due to the meadow's elevation reduced the flight time to less than 10 minutes.

Prior to the field work, the locations were found and map tiles were cached to enable a base map to be loaded when no internet connection was available. The flight was planned in the field, adjusting for conditions not visible in the satellite imagery (Figures 10, 11, and 12). The onboard GPS was used to locate the UAV on the base map. The flights were planned as transects paralleling the stream channels. Way points were selected with the stream slightly offset of center enabling some obliqueness to enhance SfM stitching while keeping the stream within the area least affected by vignetting.

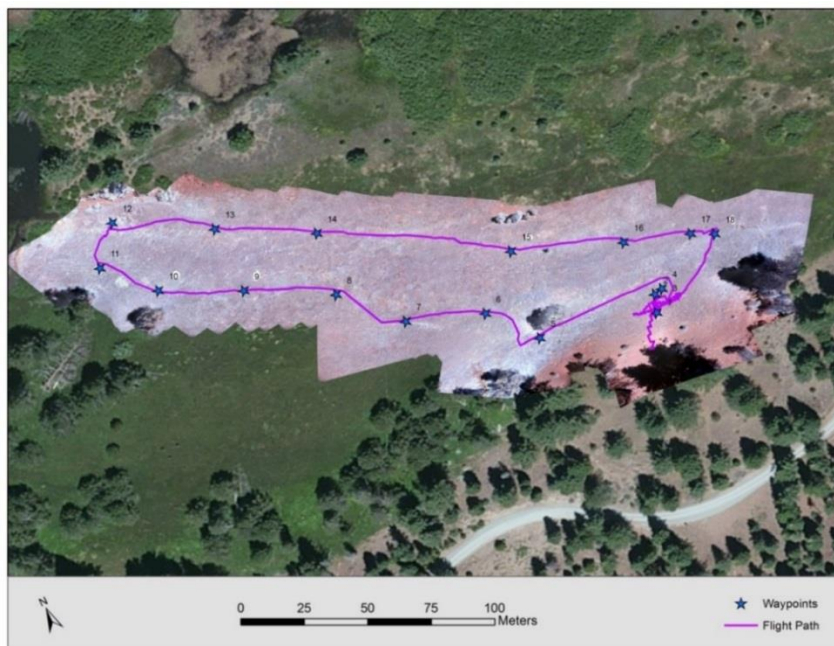


Figure 10. Knuthson flight plan on NIR mosaic. This image shows the flight path over the meadow. It is displayed on the orthomosaic which been laid on top of 0.3m resolution Digitalglobe 2010 satellite imagery.

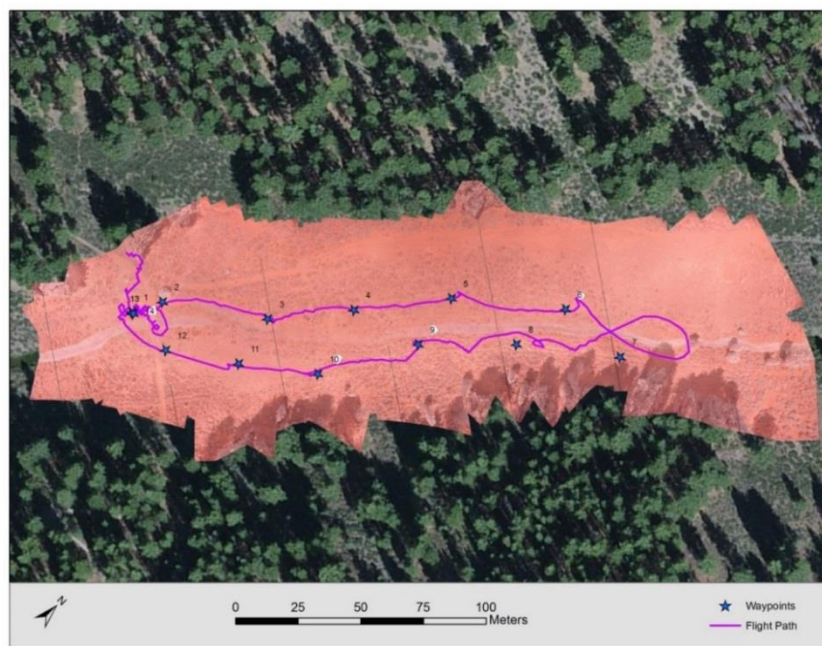


Figure 11. Dry Creek flight plan and way points with the full UAS collected CIR orthomosaic over 0.3m resolution Digitalglobe 2010 satellite imagery.

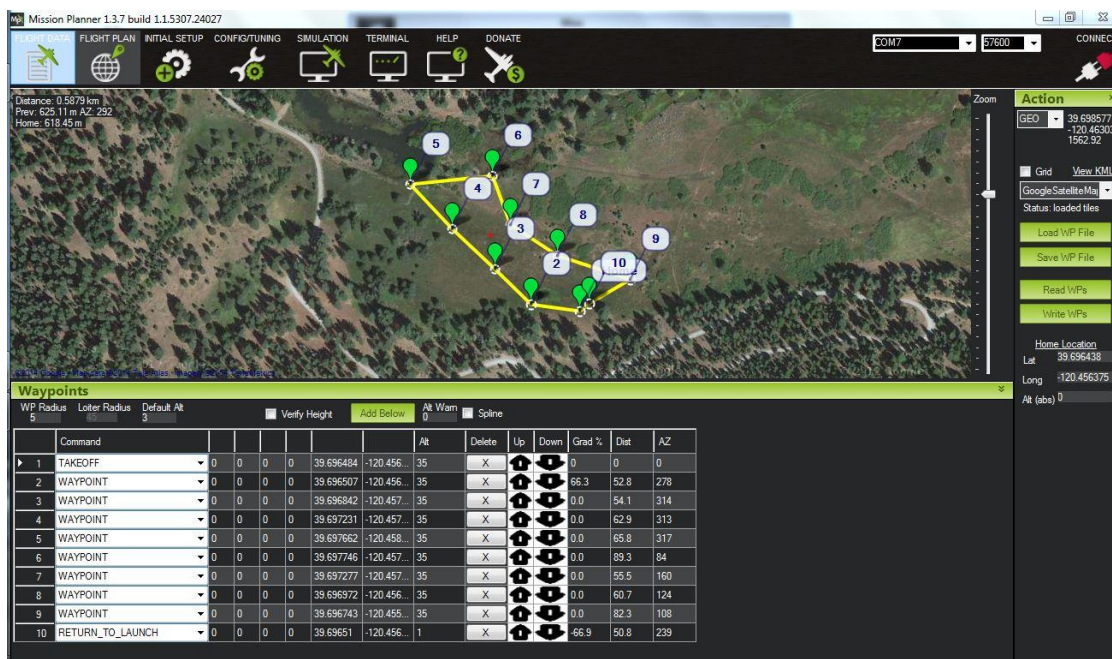


Figure 12. Example of the Mission Planner interface and Knuthson meadow flight plan.

The Canon s95 camera, modified to record NIR light, was used with a Hoya A25 red filter for all flights. Before the flight, a white balance was performed on a white piece of paper. The CHDK basic intervalometer was used with manual focus set at infinity, shutter speed at 1/1600 second, and the aperture as wide as possible. The camera was mounted at nadir and our flights at an altitude of 35m produced photos with an approximate ground sample distance (GSD) of 1cm.

Few ground control points (GCPs) were placed in the meadows. The orthomosaics used to calculate the NDVI do not require the level of accuracy that creating a DSM does. Orthophoto mosaics were created from the collected images using a SfM derived 3D surface model constructed using Agisoft's Photoscan. The NDVI was computed on both the mosaic and on individual images using ESRI's Arcmap.

Because there are no spectral response curves for the s95, and no tunable monochromatic light source was available to create our own, we decided that calculating an NDVI using a dirty red channel was our only option. To do so using a jpeg image required additional steps to get a

product that had valid NDVI values between 1 and -1 (Figure 13). Because the mosaicking process ends with the image having a large border of zero values this must first be removed. To do this the mosaic is clipped by a raster that has had its 0 values converted to null values. Then it is necessary to convert the 8 bit jpeg to 32 bit float images in preparation for division, as an 8 bit image cannot store the decimal values the NDVI outputs. Then the false red (fRed) band is created by subtracting the blue channel (pure NIR band) from red channel (red band + NIR band). To ensure the appropriate values are derived, all negative numbers are then converted to 0. Then the NDVI is calculated  $(\text{NIR} - \text{fRed})/(\text{NIR} + \text{fRed})$ . The jpeg to NDVI model can be seen in Figure 13. The mosaic was georeferenced using 2013 1 meter resolution USDA Nation Agriculture Imagery Program (NAIP) imagery to facilitate comparison. NAIP imagery is 4 band multispectral aerial imagery collected and distributed by the USDA (<https://www.fsa.usda.gov/FSA>).

## 5.4 Results

The spatial resolution of the UAS collected imagery was far superior to NAIP even though NDVI used a red band with significant NIR influence. However, radiometric differences in shade/direct sun and vignetting were significant. Attempts to perform an unsupervised classification of the image using Erdas Imagine were unsuccessful due to the very high resolution and radiometric differences between areas of sun and shade. A 10 and a 20 class unsupervised classification were attempted. Although they did successfully classify vegetation and exposed earth, they did little to differentiate between stream channel species. In addition to unsupervised classification various NDVI value thresholds were used to successfully identify the stream channel, but these value thresholds were unsuccessful in differentiating mid-channel vegetation differences. The higher density of grass in mid channel may result in more shade, which drops NDVI values. In the future, creating an ad hoc spectral library of vegetation while on the ground could be used to increase the success of image classification. Using an object-oriented approach might also improve the success of vegetation classification since the high spatial resolution of the images might allow for individual plant identification. This method—of establishing a spectral library of plants and capturing images under ambient lighting during cloudy weather--would help

to reduce the radiometric effects of shadows and allow for better analysis of the collected multispectral data.

The NDVI we calculated produced the valid results where all values fell within -1 and 1, with the wettest vegetation displaying the highest values. In the Dry Creek images, the channel is clearly visible. Additionally, the sage also responded strongly and was clearly visible. A comparison with NAIP imagery shows that although the channel is also visible in NAIP, the increased resolution of the UAV imagery provides a much more detailed view.

NVDI imagery did not satisfy the initially intended purpose. While channel detection was successful in Dry Creek, where the channel was incised and could be easily detected with conventional color imagery, the more subtle incipient channels of Knuthson Meadow could not be detected (Figures 14, 15, 16, 17, and 18). The primary reason for this is homogeneity of the vegetation and the vegetation stress in the meadow. This is likely related to the height of the water table and root access to this water. There may be a point when the root depth of the plants in the channel is sufficiently deeper than the root depth of the plants outside of the channel to cause a noticeable difference in the NDVI but we did not encounter those conditions during our survey. We did not know the height of the water table. Having that information would enable us to fine tune the time of survey to collect data when the in-channel vegetation would have better access to water and therefore a unique spectral signature.

The secondary goal of the NVDI work:--differentiating between mid-channel species in the incised channel of dry creek—was also not met. This is because the radiometric differences had a much greater effect than species difference. It must be noted that although these two goals were not met, comparing our NVDI results with the existing free NAIP data sets, proves that a consumer grade camera is capable of producing much higher resolution data, with the possibility of much more frequent revisits. In the UAV derived imagery, individual sage plants are identifiable and the stream channel can be defined with a much higher accuracy (Figures 19, 20, 21, 22, 23, and 24). Creating an ad hoc spectral library would increase the possibility of species differentiation and a better understanding of water table height might lead to an optimal time to fly to capture braided channel vegetation response.

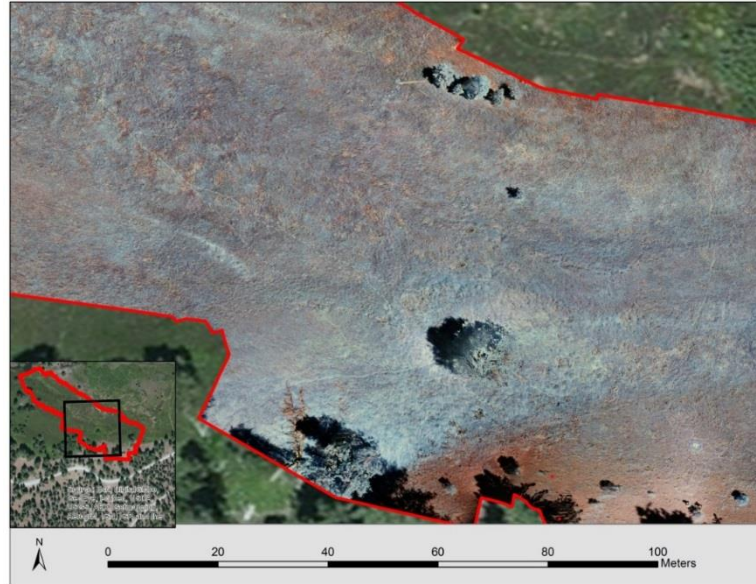


Figure 13. Knuthson UAV Unmodified 'CIR' orthomosaic against satellite imagery.

This is a close-up of the UAS collected CIR orthomosaic. It was chosen to display the level of resolution. In it we can see individual tufts of meadow grass and individual sage bushes.

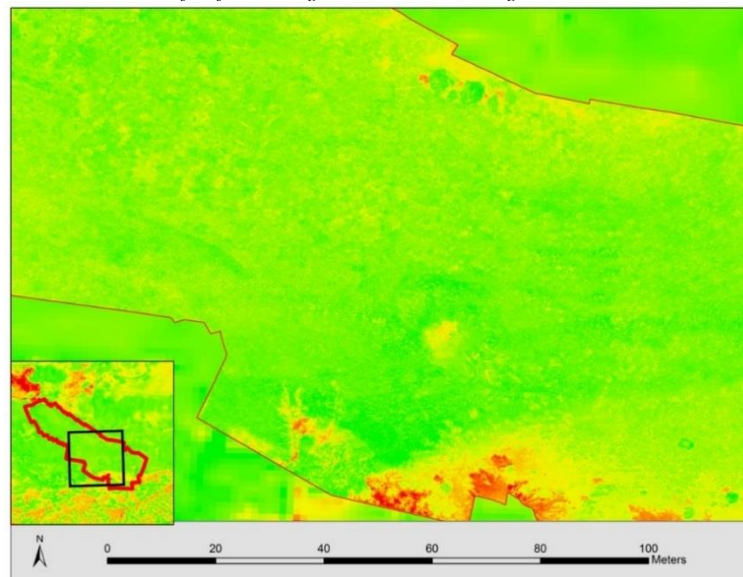
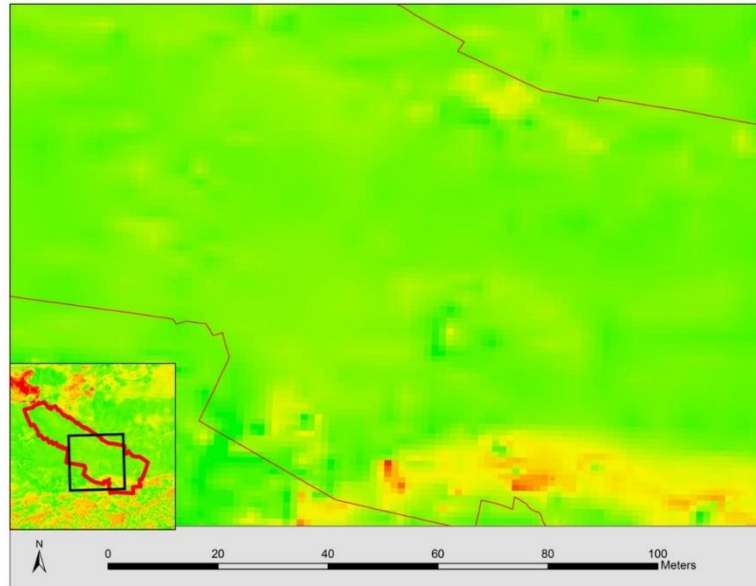


Figure 14. Knuthson UAV NDVI calculated for the same area overlaying the NAIP NDVI.

Notice that the surface of the meadow, including the willows at the top of the image and the pines and the bottom, is largely homogenous. The only major variation seen is in the shadows surrounding the trees and the dry slope and sage at the bottom of the image. Green represents high NDVI values, red represents low.



*Figure 15. Knuthson NAIP NDVI*

*This is the free 1m resolution NAIP NDVI for the same location. A comparison with figure 15 shows that the NAIP NDVI is similarly homogeneous. The comparison also reveals that the UAS collected data is much more detailed.*

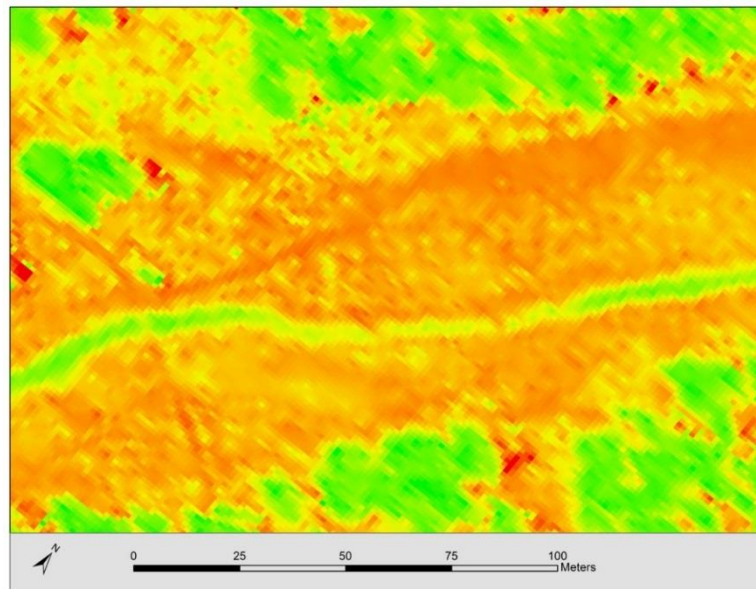


*Figure 16. Dry Creek NAIP NDVI.  
The NAIP NDVI for the same area as Dry Creek 1.*

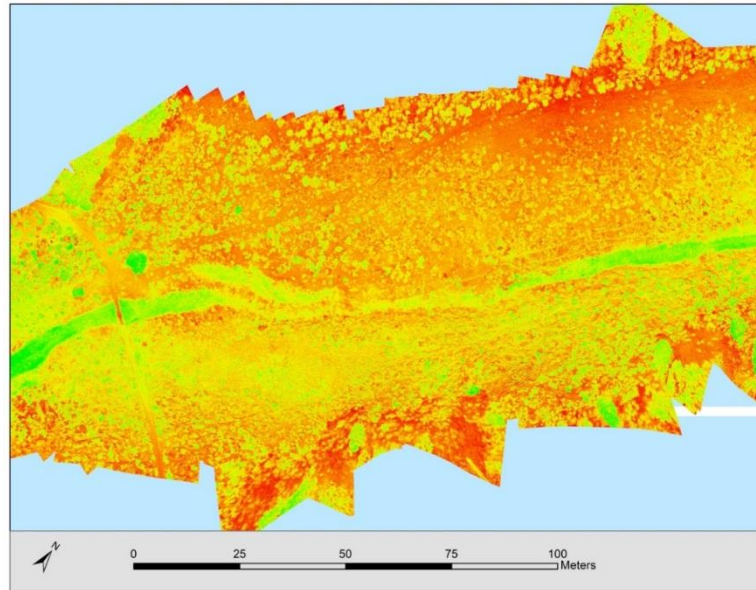


*Figure 17. Dry Creek UAV orthomosaic NDVI*

*UAS collected NDVI for the same area as above. Notice that the stream is equally well defined in both but that the increased resolution of the UAS NDVI could allow for individual plant counts.*

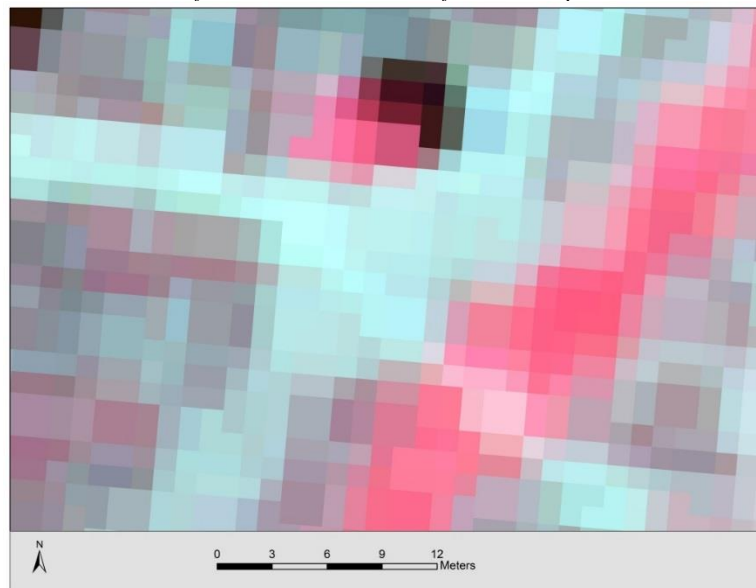


*Figure 18. The NAIP CIR image for the same area as figure 20..*

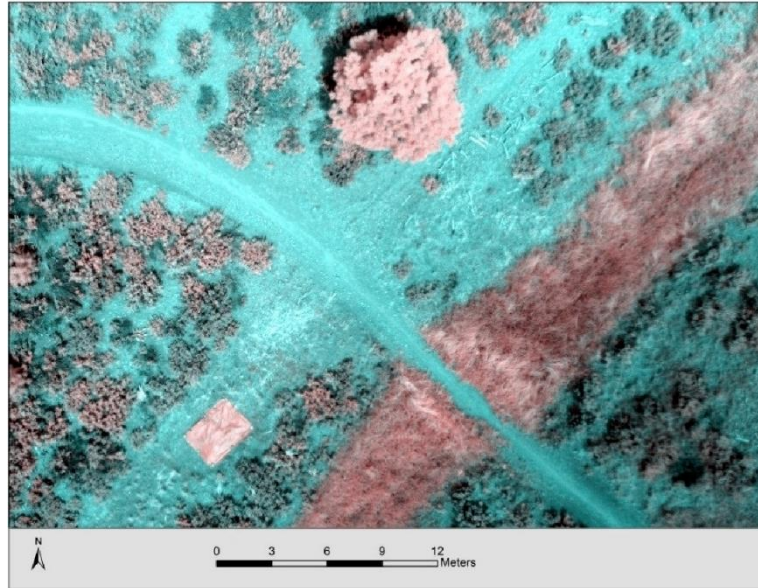


Figure 19. Dry Creek UAV single image displayed as 3-1-1 to better emulate CIR.

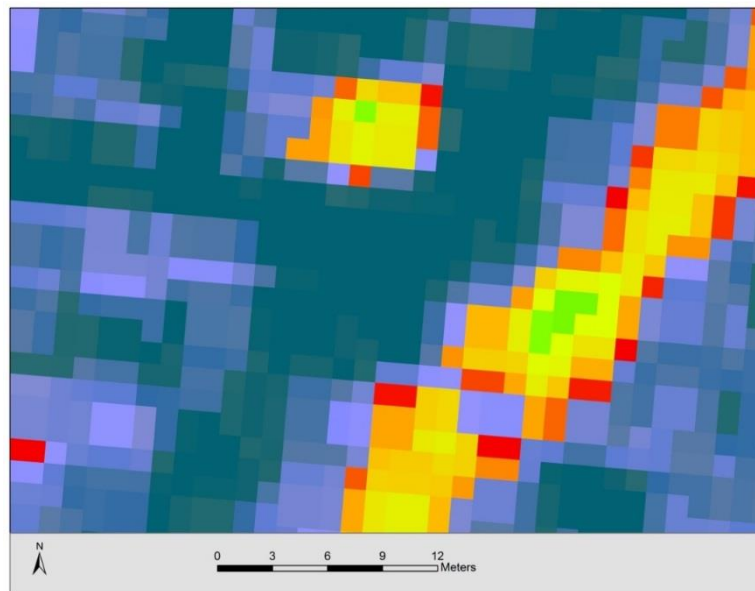


Figure 20. Dry Creek NAIP NDVI individual image area

The NAIP NDVI for the same area as Dry Creek 4. Green represents high NDVI values. Blue represents low values.

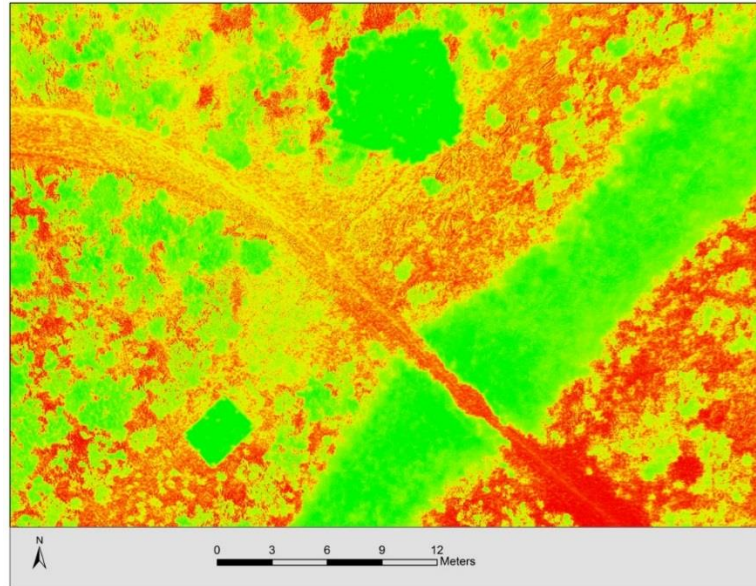


Figure 21. Dry Creek UAV single image NDVI.  
The NDVI calculated from Dry Creek 4. Notice the effect of shadow on the index, most visible around the pine tree in the top of the image. Green represents high NDVI values. Red represents low values.

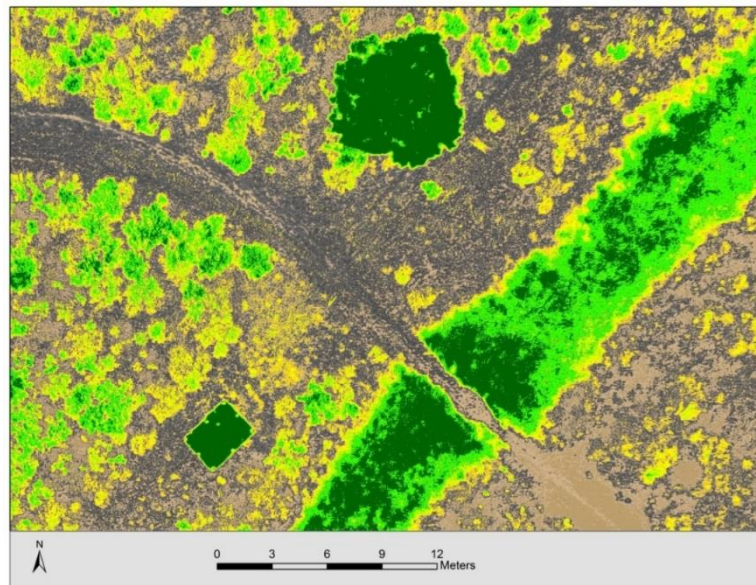


Figure 22. Dry Creek 8a: unsupervised classification with 10 classes

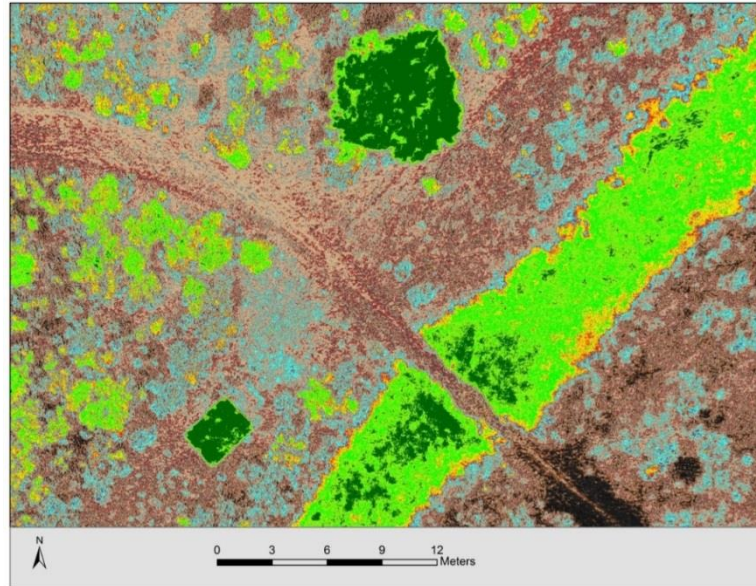


Figure 23. Dry Creek 8b: unsupervised classification with 20 classes

## Chapter 6: Gullies

### 6.1 Introduction

The development of a hillslope gully degrades useful land, threatens infrastructure, and pollutes water bodies with fine sediment. These gullies are the result of erosion due to concentrated flow and can occur in a variety of soils including sandy soils, soils that form a crust such as loess, and in soils where piping exists. They typically deepen until a resistant soil layer is reached at which point they widen until an equilibrium is reached. Gullies begin with a headcut that moves upslope at a rate depending on various factors including soil type, angle of slope, and discharge rate. Gully widening actions are very similar to those seen in landslides, with vertical gully walls undergoing failure during rainfall events especially where there is little stabilizing vegetation cover. Research and monitoring of gullies has historically been hampered by the difficulties in accurately measuring rates of erosion caused by gullies' unique topography and scale (Valentin et al., 2005; Wells et al. 2013).

A gully's sediment loss occurs via horizontal and vertical enlargement while its storage is evident as a decrease in depth. Because gullies may often be deeply incised with nearly vertical

sidewalls, monitoring their boundaries in orthophotos provides little information regarding the amount of sediment being lost or stored over time. It is possible to measure the horizontal expansion of a gully in orthophotos but not the vertical change. In order to model and monitor hillslope gullies one must be able to measure volumetric change. Publicly available elevation data sets rarely capture all but the largest interior features of gullies and their revisit rate is too slow to monitor seasonal change.

Casalí et al. (2006), whose research incorporated a set of gullies, demonstrated the inadequacy of manual measurement methods, deriving gully volume by creating cross sections at set intervals, using survey tapes and a micro-topographic profile meter. They found that as the cross section interval and the precision of the measurement increased, the error decreased. This fact combined with the large and random error at all scales and methods exposes the need for an alternative measurement method that is not dependent on cross section sampling (Casalí et al., 2006).

Perroy et al. (2010) used terrestrial LiDAR to map gullies on Santa Cruz Island off the coast of California. They found most common sources of surface data, especially U.S. National Elevation Dataset (NED) elevation models, are of insufficient resolution to effectively calculate the volume of gullies. They acknowledged the high cost of aerial LiDAR and tested tripod-mounted terrestrial laser scanning (TLS). They found that an available aerial LiDAR point density of  $1/m^2$  resulted in underestimation of gully volume. They found however that the side looking orientation of TLS produced significant topographic shadows which resulted in an even more severe underestimation of gully depth (Perroy et al., 2010).

Very high resolution and accurate surface data are needed to effectively monitor gullies. The potential to capture very high resolution elevation at fast revisit rates, coupled with the ability to capture extremely steep sidewalls, make a low-altitude UAV photography and SfM modeling method a promising choice for gully survey. With attention to coordinate systems and monumentation used to place ground control points, this method has the potential to deliver the necessary surface models needed to monitor gully formation and expansion.

## 6.2 Study Site

Gullies are formed along elevated coastal terraces in coastal San Mateo County, California, typically on soils on geologic units that weather to smectite clays (Swanson et al., 1989) and clay-rich coastal terrace deposits, but are enhanced in areas of agricultural expansion on hillslopes (Davis & Sims, 2013). Vegetation communities associated with these hillslope gullies are grass and coastal scrub. Gullies expand via piping networks focused near the base of the A horizon of mollisols (Swanson et al., 1989), with piping initiated by burrowing rodents such as gophers. In some instances, gullies cut into clay-rich soils can develop extremely steep sidewalls approaching vertical in some areas.

We selected a gully (Figure 25) in Pacifica, California, with extremely steep side walls and complex internal interfluvial and channel networks that provides difficult challenges for survey and surface modeling. Gully surfaces were primarily bare soil with patches of pampas grass (*Cortaderia selloana*) and an occasional small pine tree (*Pinus radiata*) growing between interfluvial areas. The adjacent hillslopes were vegetated with small woody shrubs (dominated by *Baccharis pilularis*) and grasses. There were several mature pines and larger shrubs growing at the foot of the gully. The gully was chosen as a study site to support sediment source analysis of the watershed containing similar gullies (Davis & Sims, 2013). The gully, located on a southeast facing ~35% slope in Pacifica, CA, is up to 6 meters deep in cross section, 50m long and 20m wide for the area of interest. This area is defined as beginning at the upslope start of the gully and running down until an intersection with a smaller tributary gully on the eastern side. Attempts to survey this feature in the past have met with great difficulties, with conventional survey methods only possible by potentially erosion-enhancing methods (if internal features are to be occupied using a stadia or prism rod), and the internal structure not observable from gully side sites suitable for setting up a total station or terrestrial laser scanner.



*Figure 24. Photograph taken from head of gully, illustrating typical land cover of bare gully subsoils, pampas grass, juvenile and mature evergreen trees, and herbaceous vegetation on ungullied hillslopes surrounding the cut.*

### **6.3 Methods**

While the gully survey presents challenges for conventional survey, its relatively small size meant that it would be straightforward to select a combination of platform and camera. The size of the study site meant that a helicopter configuration, specifically a multi-rotor system, would not present challenges of battery life, and would provide advantages of stability, reliability, and vertical flight patterns.

Before flying, 22 GCPs were surveyed using a Leica 3-second total station starting from a temporary ground stake monument positioned using a Trimble GeoXH 6000 GNSS unit. A distant feature identified on existing orthophotos was used to establish a backsight direction for the total station coordinate reference in UTM Zone 10, WGS 1984. Four GCPs were crosses

made of 1m sections of 1” (2.54cm) PVC piping arranged in an ‘+’ with black electricians tape. Six were white ceiling tiles with a ‘+’ of electrician's tape and a compact disk (CD) in the center. An additional twelve GCPs were unaltered CDs.

Flights were planned at altitudes of 10, 20, and 70m above the launch site with predicted pixel sizes of approximately 3mm, 6mm and 2cm respectively (table 6). Camera settings were set manually to ISO 125, shutter speed 1/600 second, aperture f/2.2, and focal length of 6 mm (equivalent to a 28 mm focal length for a standard 50 mm camera). The CHDK intervalometer program was used to capture photographs at a three-second interval. The flight conditions were windy but this did not result in images far from nadir. Skies were overcast which resulted in excellent lighting conditions for the gully, with few shadows. The bottom of the gully was however somewhat dark. In the future RAW format images could be used or gamma correction could be applied to increase the possibility of matches in these areas.

Flight elevation range	Min GSD (cm/pixel)	Max GSD (cm/pixel)	Ortho-photo resolution (cm)	DSM resolution (cm)	Number of Images	Mean height AGL (m) from Photoscan	Photo overlap along flight path (number of photo pairs)	Photo overlap between flight paths (number of photo pairs)
10m-30m	0.28	0.84	0.75	1.5	25	27.60	55% (8)	59% (4)
20m – 40m	0.56	1.13	1.0	2.0	34	33.06	62% (10)	62% (6)
70m – 90m	1.97	2.53	2.5	5.0	24	70.22	85% (3)	NA

*Table 5. Flight altitudes above ground level (AGL), ground sample distance (GSD), and overlap measured from photographs including in parentheses the number of photo pairs used in the measurements.*

Ground surface distance (GSD) was calculated using the mission planner's flight planning interface. The minimum and maximum altitudes above ground level (AGL) were 10 and 90 meters. The flight was level rather than following the slope. The flight planning waypoints should be considered the lowest altitude AGL. At the lower end of the gully an additional ~20m must be added to the altitude to account for the slope.

Flights were planned with up to four transects running parallel to the gully slope (fig. 26). The takeoff and landing site was upslope at an 18m distance from the head of the gully. This site was chosen for gradual slope and distance from scrub vegetation, in order to reduce the difficulty and danger on take-off. The GPS does not offer sufficient precision for automated landing avoiding scrub and steeper areas, so the landing was performed manually.

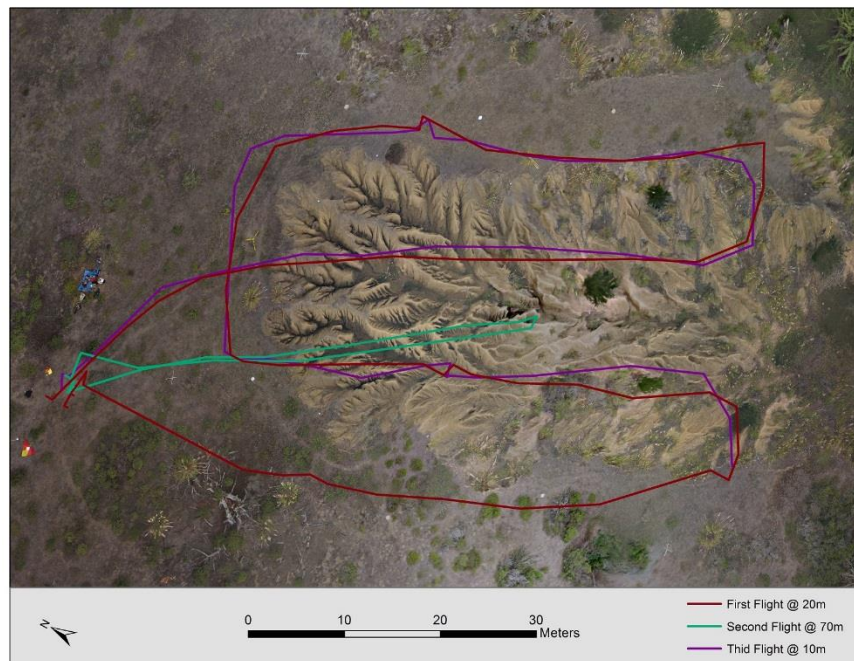


Figure 25. Three successive flight paths, with heights above launch pad of 10, 20 and 70 m.

## 6.5 Image Processing Results & Analysis

After culling unusable photography resulting from blurriness or during takeoff and landing, 25, 34 and 24 photographs were compiled from the three flights (see table 6). Using overlapping image tools of a photo-editing program, Paintshop Pro 7.0, overlap was measured between successive pairs of photographs, and between adjacent flight lines. The goal was >60%

overlap following standard photogrammetric practice for stereo pairs, and this was achieved for the 20m and 70m flight, but the last and lowest flight had less than 60% overlap (see table 6).

Four models were attempted using the imagery and GCPs using Agisoft Photoscan Professional, from each of the nominal 10m, 20m and 70m flights, and from a combination of all imagery. Settings for accuracy and density were set to the highest possible values, and camera parameters were optimized according to software guides. The GCPs were identified manually in the images and associated with coordinates from the total station. Outputs included orthophoto mosaics (fig. 27) and a georeferenced DSM (fig. 28).



*Figure 26. Section of orthomosaic (originally in color) created from 20m flight, 33m average altitude above ground level (AGL), 34 photographs.*

All three types of GCPs were sufficiently visible to tag in imagery at all heights, though crossed PVCs were the most visible. The CDs' high level of reflectivity and round geometry led to some distortion both in color and shape at low resolutions on the 70m flights and at the bottom of the gully on the 20m flights. The ceiling tiles were the most difficult to work with, but could be improved by using a wider black tape target. However, the large square might be an excellent option in thick grasses found in meadows as it would increase the visibility of the GCP by pressing down a large swath of the grass.



Figure 27. Digital Surface Model of 20m (33m average altitude AGL) Model derived from structure-from-motion methods employing Agisoft Photoscan. Contour interval: 0.2m. Index contours: 1m.

Table 7 gives the results of error analysis for the models generated from the three flights. Root-mean-squared-error (RMSE) estimates of each model, using all available GCPs, were derived from a report generated by the software. We used a leave-one-out cross validation method in order to determine how well the model fit check points not used in the model, and refit the model for each of the GCPs. Two additional sets of RMSE results are produced from these multiple fits, one estimate from all of the leave-one-out models, the other the cross-validation RMSE from the checkpoint errors. The cross validation results are probably the best measure of model fit. For all models, we observed that the overall cross-validation error gets most of its contribution from Z errors. The lowest errors are not surprisingly from the lowest mean height above ground level (AGL): 0.0566m for the 27.60m average AGL flight, however this group of photographs did not have sufficient overlap for the model to cover the head of the gully. Errors for the two higher flights are remarkably close, despite the great different in height AGL of image capture: 0.0836m for the 33.06m models and 0.0904m for the 70.22m models. Notably, the model built from all 83 photographs has the highest error -- 0.125m -- suggesting that maintaining a relatively consistent scale of photography may be advantageous.

## **6.6 Discussion**

To determine the suitability of SfM data, we can compare its surface model and orthophotography with available data. While color orthophotography is available at increasingly finer resolutions, especially in urban areas, the resolution achieved in our gully survey, to ~1cm pixels for the 33m flight, is far finer than any currently available from public sources. Similarly, the digital surface model, based on a point density of over 2000 per square meter, is orders of magnitude finer than the best public data from LiDAR, at 3.4 points per square meter for the Golden Gate LiDAR project (GGLP), flown in 2010. This is not surprising as the GGLP data covers multiple counties. Our SfM results are more comparable to fine-scale studies employing either total-station topographic surveys, terrestrial laser scanning, or contracted low-altitude LiDAR.

Model	GCPs Used	X error (m)	Y error (m)	Z error (m)	Overall error (m)
<b>10m (27.60m mean AGL) flight</b>					
Model, all GCPs	14	0.0205	0.0233	0.0344	0.0464
RMSE of all leave-one-out models	13	0.0205	0.0232	0.0341	0.0460
Check point error cross-validation RMSE	1 check-point each, 14 models	0.0231	0.0270	0.0440	0.0566
<b>20m (33.06m mean AGL) flight</b>					
Model, all GCPs	14	0.0131	0.0174	0.0658	0.0693
RMSE of all leave-one-out models	13	0.0131	0.0173	0.0652	0.0687
Check point error cross-validation RMSE	1 check-point each, 14 models	0.0156	0.0199	0.0683	0.0836
<b>70m (70.22m mean AGL) flight</b>					
Model, all GCPs	22	0.0245	0.0223	0.0747	0.0817
RMSE of all leave-one-out models	21	0.0244	0.0223	0.0745	0.0815
Check point error cross-validation RMSE	1 check-point each, 22 models	0.0277	0.0241	0.0826	0.0904
<b>All flights combined</b>					
Model, all GCPs	22	0.0163	0.0229	0.1097	0.1132
RMSE of all leave-one-out models	21	0.0163	0.0228	0.1093	0.1128
Check point error cross-validation RMSE	1 check-point each, 22 models	0.0186	0.0257	0.1250	0.1290

Table 6. Root-Mean Square Error (RMSE) estimates for models.

The gully's location included in the GGLP allowed us to compare our product with an industry standard data set (table 8) contracted by the US Geological Survey for 1/9 arc second (3 m in projected UTM coordinates) National Elevation Dataset (NED) data, as well as with a digital surface model created from first returns of the original LiDAR data used for that contract, from the Golden Gate LiDAR project (Hines, 2011). The comparison immediately revealed several interesting differences (fig. 30). The most immediate was the lack of internal gully interfluves included in the (GGLP-derived) bare earth NED elevation raster. The process of classifying the point returns resulted in all the internal gully interfluves being labeled as medium vegetation. Once the medium vegetation points were included, the GGLP dataset produces a DSM similar to the SfM dataset, though far less detailed, and both including vegetation.

33.06m SfM DSM: Cross-validation	2010 Golden Gate LiDAR Project DSM
RMSE X (cm) = 1.56	Horizontal RMSE (cm) = < 100
RMSE Y (cm) = 1.99	
RMSE Z (cm) = 6.83	Vertical RMSE (cm) = < 9.25
Point density: 2374.54 points per sq meter	Point Density 3.4 points per square meter

Table 7. Comparison of SfM and Golden Gate LiDAR Project DSMs.

After the creation and georeferencing of the SfM derived DSM an attempt was made to calculate the volume and area difference between 3 datasets: the 3m NED, the GGLP first-return DSM, and the SfM derived DSM (table 9). A minimum eroded volume process was used to determine gully volume. This process uses a 'cap' constructed over the top of the gully from which the underlying gully is subtracted resulting in volume. The cap was derived by creating a TIN from the vertices of a gully boundary line. This line was determined using an analysis of change in slope. An abrupt break in slope was identified as the gully boundary. The line was verified and cleaned before being converted to points. The bottom border of the gully was constructed using an arbitrary line drawn between features visible in all three datasets.

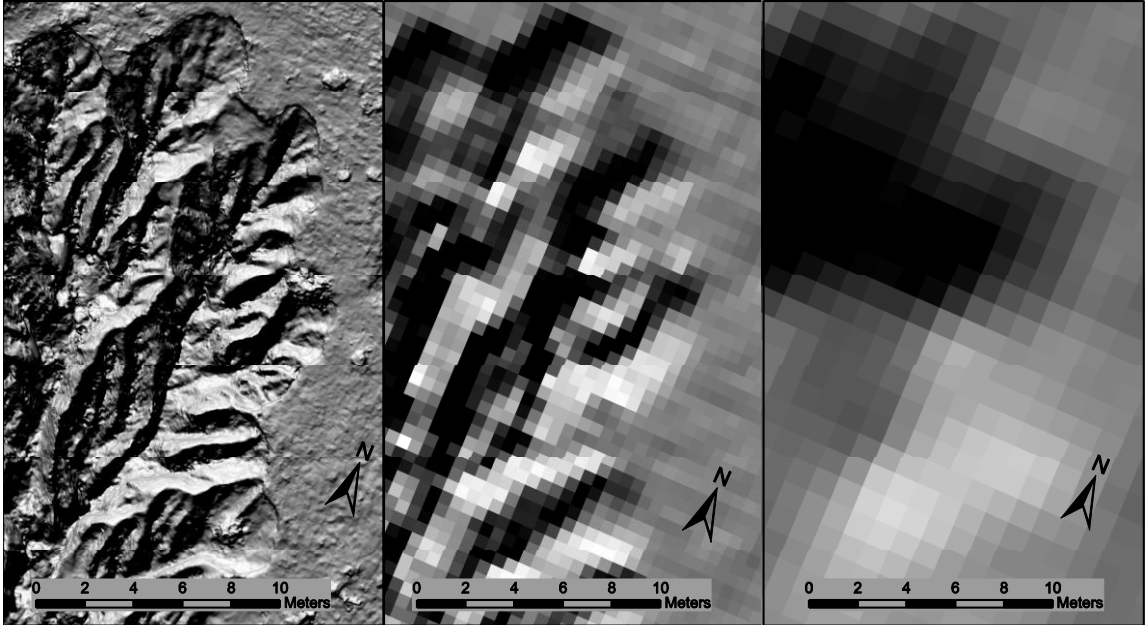


*Figure 28.* Comparison of digital surface model (DSM) generated using structure-from-motion methods from the 20m flight photography (left) with a 50cm DSM generated from first returns of the Golden Gate LiDAR Project (center) and a 1/9 arc second National Elevation Dataset elevation model interpolated to 1m cells (right).

Dataset	Volume (m <sup>3</sup> )	Area (m <sup>2</sup> )	Cell Size (m <sup>2</sup> )
USGS DEM	4507.58	1298.00	1
SfM DSM	3908.18	1255.93	~0.034
GGLP DSM	3532.81	1172.56	0.5

Dataset Difference	Volume Difference (m <sup>3</sup> )	% of USGS vol	% of GGLP vol	% of SfM vol
USGS-GGLP	974.78	21.63%	27.59%	n/a
SfM - GGLP	375.38	n/a	10.63%	9.60%
USGS-SfM	599.40	13.30%	n/a	15.34%

Dataset Difference	Area Difference (m <sup>3</sup> )	% of USGS area	% of GGLP area	% of SfM area
USGS-GGLP	125.44	9.66%	10.70%	n/a
SfM - GGLP	83.37	n/a	7.11%	6.64%
USGS-SfM	42.07	3.24%	n/a	3.35%

*Table 8. Volumetric and areal comparisons of SfM with USGS and GGLP DSMs.*

The analysis provides evidence for gully growth over the three years between when the LiDAR was collected and when the hexacopter survey was flown. The SfM DSM has greater volume and area than the LiDAR-derived DSM. A visual comparison with the 3m NED demonstrates the poor suitability of publicly available elevation datasets for gully analysis, however accurate comparisons are limited. Attempts to look at spatial patterns of dataset

differences yield patterns related more to difference in resolution and the difficulties of accurate registration where extremely steep-sided interfluves may be centimeters wide. Furthermore, since the NED dataset is derived from the LiDAR, the effect of the vegetation ‘cleaning’ algorithm on finely detailed gully features is likely significant. Since the SfM-derived DSM is also affected by vegetation, improvements should be considered such as using automated classification and masking methods to approach a bare earth model: masked vegetation could potentially be smoothed to the level of the surrounding surface.

The fine-resolution results of the gully survey opens up a use for studying geomorphological processes. Features such as piping inflows, measured in centimeters are visible in SfM-derived orthophotography and elevation models. The connections between rodent burrows, piping and gully expansion observed by Swanson et al. (1989) can be studied in repeated surveys. If care is taken to monument surveys, repeats in successive years can be used to document sediment yield volumes and improve gully growth models. .

## **Conclusion**

This study tested the viability of a very low cost UAS as a data collection platform for environmental science and geomorphological research by comparing free and common data against that produced using the UAS. Two methods were used in this study, creating a DSM using SfM and calculating the NDVI using a modified consumer camera. SfM was used to create a DSM of hillslope gullies near Pacifica, California. The NDVI was calculated for orthomosaics of montane meadows in the Sierra Nevada Mountains of California.

The UAS comprises a 3D Robotics hexacopter, an Ardupilot Mega autopilot control board, a laptop and two Canon S95 digital cameras, one modified to record non-visible wavelengths. The hexacopter was chosen because it provides a stable camera platform, allows for vertical and nonlinear flight paths, and has redundancy to protect against motor failure. The cameras were chosen based on their low weight, large sensor size, compatibility with CHKD, reasonable cost, and availability as a NIR converted camera.

The SfM method determines the 3D coordinates of features matched between overlapping images. With a sufficient number of overlapping images we were able to create a

very dense DSM using Agisoft's Photoscan that was georeferenced using ground control points. The NDVI was calculated using the blue and red channels. The camera's hot mirror was removed, allowing all channels to record NIR and UV bands. A highpass Hoya A25 red filter ensured that the blue channel recorded only the NIR band while the red channel recorded both red and NIR bands. The value from the blue channel was subtracted from the red to create a false red band, this allowing capture of near infrared imagery that is useful in determining various aspects of vegetation.

This research shows that with careful attention to requirements of overlap and monumentation unchanged from existing principles of photogrammetry, it is possible to collect data suitable for gully geomorphometry with a very low cost UAV and consumer-grade compact camera. These methods may also provide data currently unattainable using currently available methods, including terrestrial laser scanning, due to the unique perspective of low-altitude flights. The surface model is much denser than available LiDAR data, meaning that features such as piping inflows created by burrowing animals are detectable, increasing our ability to study the distribution of features significant to geomorphic process. The inability to penetrate taller vegetation however means that this technology will never replace LiDAR. Under conditions of mostly bare soils and minimal vegetation height, however, SfM appears to be a good, low-cost solution for mapping small erosional features such as hillslope gullies and monitoring their growth.

This research also shows that using consumer grade cameras converted to multispectral sensors has great promise for detecting small, obscured montane meadow stream channels but the method requires further development. The attempt to identify subtle incipient and ephemeral stream channels was largely a failure. The spectral resolution of the multispectral data from the modified Canon s95 was not sufficient to identify the in-channel vegetation, as radiometric differences proved to be much greater than variation in vegetation stress levels. However, we believe that there is much room to improve upon this method through the use of better filters and raw format data, the creation of local spectral libraries of vegetation, and timing the collection of data for times when the light source is more ambient. However, compared to the use of NAIP imagery, the centimeter level resolution and low cost for rapid repeat visits of the UAS may

justify UAS use in montane meadow stream monitoring, especially with the improvements in equipment and methods noted above.

## References

3D Robotics, <http://3drobotics.com/>

Aber, J.S., Marzloff, I., and Ries, J., 2010. *Small-Format Aerial Photography: Principles, Techniques and Applications*. Elsevier.

Adams, J., Parulski, k., and Spaulding, K., 1998. Color processing in digital cameras. *IEEE micro* 18, no. 6, 20-30.

Akay, A. E., O?uz, H., Karas, I. R., & Aruga, K., 2009. Using LiDAR technology in forestry activities. *Environmental monitoring and assessment*, 151(1-4), 117-125.

Allen-Diaz, B. H., 1991 Water Table and Plant Species Relationships in Sierra Nevada Meadows. *American Midland Naturalist*, 126.1, 30-43.

Ambrosia, V. G. & Zajkowski, T., 2012. Selection Of Appropriate Class UAS / Sensors To Support Fire Monitoring: Experiences In The U.S.

Ashraf, M., Maah, M., and Yusoff, I., 2011. Remote Sensing of Biomass, Biomass and Remote Sensing of Biomass, Dr. Islam Atazadeh Ed., ISBN: 978-953-307-490-0, InTech, DOI: 10.5772/16462. Available from: <http://www.intechopen.com/books/biomass-and-remote-sensing-of-biomass/introduction-to-remote-sensing-of-biomass>

Bennett, M. J., and Wheeler, F. B., 2010 Raw as archival still image format: A consideration. In *Archiving Conference*, vol. 2010, no. 1, 185-193. Society for Imaging Science and Technology.

Bento, M. D. F., 2008. Unmanned aerial vehicles: an overview. *Inside GNSS*, 3(1), 54-61.

Biasio, M., Arnold, T., Leitner, R., McGunnigle, G., and Meester, R., 2010. UAV-based environmental monitoring using multi-spectral imaging. In *SPIE Defense, Security, and Sensing*, , 766811-766811. International Society for Optics and Photonics.

Blumberg, D. , Neta, T. , Margalit, N. , Lazar, M. , & Freilikher, V., 2004. Mapping exposed and buried drainage systems using remote sensing in the Negev desert, Israel. *Geomorphology*, 613, 239-250.

Bosak, K., 2012. Secrets of UAV photomapping. Technical report, Pteryx UAV by Trigger Composites.

Casalí, J., Loizu, J., Campo, M.A., De Santisteban, L.M., Álvarez-Mozos, J., 2006. “Accuracy of methods for field assessment of rill and ephemeral gully erosion.” *Catena*, vol. 67, no. 2, 128–138.

CHDK, <http://chdk.wikia.com/wiki/CHDK>

Cheng, T. , Riano, D. , Koltunov, A. , Whiting, M. , Ustin, S. , et al., 2013. Detection of diurnal variation in orchard canopy water content using modis/aster airborne simulator (MASTER) data. *Remote Sensing of Environment*, 132, 1-12.

Christian, P., Davis, J., Blesius, L., 2013. Application of a very-low-cost unmanned aerial vehicle (UAV) and consumer grade camera for the collection of research grade data: preliminary findings – American Geophysical Union Fall Meeting (San Francisco). Dec. 12, 2013.

Curtin, D., 2007 “The Textbook of Digital Photography”. 2nd Edition. Marblehead, Shortcourses.com.

Darrouzet-Nardi, A. , D’Antonio, C. , & Dawson, T., 2006. Depth of water acquisition by invading shrubs and resident herbs in a Sierra Nevada meadow. *Plant and Soil*, 2851, 31-43.

Davis, J., Sims, S., 2013. Physical and maximum entropy models applied to inventories of hillslope sediment sources – *Journal of Soils and Sediments* 13(10): 1784-1801. DOI: 10.1007/s11368-013-0774-3.

Debinski, D., Jakubauskas, M., Kindscher, K., 2000. Montane Meadows as Indicators of Environmental Change. *Environmental Monitoring and Assessment*, 64.1, 213-225.

Digital Bolex, <http://www.digitalbolex.com/global-shutter/>

DPRReview, <http://www.dpreview.com>

Dworak, V, et al., 2013. Strategy for the development of a smart NDVI camera system for outdoor plant detection and agricultural embedded systems. *Sensors* 13, no. 2 , 1523-1538.

Edmund Optics, <http://www.edmundoptics.com/>

Eisenbeiß, H. 2009. UAV Photogrammetry. PhD Dissertation/Eisenbeiss, H., 2009. UAV Photogrammetry. DISS. ETH NO. 18515. Institute of Geodesy and Photogrammetry, ETH Zurich, Switzerland.

EO-1 satellite, <http://eo1.usgs.gov/>

Fonstad, M. , Dietrich, J. , Courville, B. , Jensen, J. , & Carbonneau, P., 2013. Topographic structure from motion: A new development in photogrammetric measurement. *Earth Surface Processes and Landforms*, 384, 421-430.

Fraser, B., 2004. Understanding digital raw capture. Digital camera raw file support, Adobe Systems Incorporated.

Hines, E., 2011. Final Report: Golden Gate LiDAR project – San Francisco, California: San Francisco State University, 12p.

Hinkley, E. A., V. G. Ambrosia, and S. Wegener. 2013 Unmanned Aircraft Systems in Environmental Monitoring Applications. In Society of American Engineers International (SAEI). (in editing)

Hoya Filters, <http://www.hoyafilter.com/hoya/products/coloredfilters/25ared/> accessed 12/18/2014

Hugenholtz, C.H., Whitehead, K., Brown, O.W., Barchyn, T.E., Moorman, B.J., LeClair, A., Hamilton, T., 2013. Geomorphological mapping with a small unmanned aircraft system sUAS.:

feature detection and accuracy assessment of a photogrammetrically-derived digital terrain model. *Geomorphology*, doi: 10.1016/j.geomorph.2013.03.023

ImageJ, <http://imagej.nih.gov/ij/>

James, M. , & Robson, S., 2012. Straightforward reconstruction of 3d surfaces and topography with a camera: Accuracy and geoscience application. *Journal of Geophysical Research-earth Surface*, 1173, doi:10.1029/2011JF002289, in press.

Kawamura, S. 1998, Capturing images with digital still cameras. *Micro*, IEEE 18, no. 6, 14-19.

Knoth, C., Klein, B., Prinz, T., and Kleinebecker, T., 2013. Unmanned aerial vehicles as innovative remote sensing platforms for high-resolution infrared imagery to support restoration monitoring in cut-over bogs. *Applied Vegetation Science* 16, no. 3, 509-517.

Laliberte, A. S., Goforth, M. A., Steele, C. M., & Rango, A., 2011. Multispectral remote sensing from unmanned aircraft: Image processing workflows and applications for rangeland environments. *Remote Sensing*, 3(11), 2529-2551.

Landinfo, <http://www.landinfo.com/satellite-imagery-pricing.html> accessed 12/16/2014

Lebourgeois, V., Bégué, A., Labbé, S., Mallavan, B., Prévot, L., & Roux, B., 2008. Can commercial digital cameras be used as multispectral sensors? A crop monitoring test. *Sensors*, 8(11), 7300-7322.

Litwiller, D. 2001. CCD vs. CMOS. *Photonics Spectra* 35, no. 1, 154-158.

Loheide, S. , Deitchman, R. , Cooper, D. , Wolf, E. , Hammersmark, C. , et al., 2009. A framework for understanding the hydroecology of impacted wet meadows in the Sierra Nevada and Cascade ranges, California, USA. *Hydrogeology Journal*, 171, 229-246.

Lu, Y. M., Fredembach, C., Vetterli, M., & Susstrunk, S., 2009. Designing color filter arrays for the joint capture of visible and near-infrared images. In *Image Processing (ICIP), 2009 16th IEEE International Conference on* (pp. 3797-3800). IEEE.

Maxmax, <http://www.maxmax.com>

Nackaerts, K., Delauré, B., Everaerts, J., Michiels, B., Holmlund, C., Mäkynen, J., & Saari, H., 2010. Evaluation of a lightweight UAS-prototype for hyperspectral imaging. *International Archives of Photogrammetry, Remote Sensing and Spatial Information Sciences, Part, 5*, 478-483.

NAIP Imagery, <https://www.fsa.usda.gov/FSA/apfoapp?area=home&subject=prog&topic=nai>

NED (2014). U.S. National Elevation Dataset – U.S. Geological Survey. <http://ned.usgs.gov>. Last modified 15-Apr-2014.

Neumann, K. J., 2008. Trends for digital aerial mapping cameras. *Int. Arch. Photogram. Rem. Sens. Spatial Info. Sci.(ISPRS)*, 28, 551-554.

Olsen, H., 2009. *Soil and Vegetation Characteristics of Montane and Subalpine Wet Meadows, Sierra Nevada, California*. n.p , ProQuest, UMI Dissertations Publishing.

Perroy, RL, Bookhagen B, Asner G, and Chadwick OA, 2010. Comparison of gully erosion estimates using airborne and ground-based LiDAR on Santa Cruz Island, California. *Geomorphology* 118: 288–300

Peterson, D. L., Jakubauskas, M. E., Kindscher, K., & Debinski, D., 2001. Hyperspectral remote sensing of nonforested montane vegetation communities. In 3rd international conference on geospatial information in agriculture and forestry, 5-7.

Photoscan: [www.agisoft.ru](http://www.agisoft.ru)

Publiclab, <http://www.publiclab.org/>

Rabatel, G., Gorretta, N., & Labbé, S., 2011. Getting NDVI spectral bands from a single standard RGB digital camera: a methodological approach. In *Advances in Artificial Intelligence* (pp. 333-342). Springer Berlin Heidelberg.

Rabatel, G., Gorretta, N., & Labbé, S., 2012. Getting simultaneous red and near infrared bands from a single digital camera for plant monitoring applications. In CIGR-Ageng 2012. International Conference on Agricultural Engineering.

Reyes, J. A. 2013. The 'secret garden': microphytobenthic biofilms and the foraging ecology of calidridine sandpipers. PhD diss., Science: Biological Sciences Department.

Sloan, J. "Creating Normalized Difference Vegetation Index NDVI. From UAS - Color Infrared Imagery Using Fiji ImageJ".

<http://rimgsc.cr.usgs.gov/UAS/pdf/imageProcessing/UAS%20Data%20Processing%20Fiji%20ImageJ%20NDVI.pdf>. July 2013. USGS

Slocombe, Michelle L., and Jerry D. Davis. 2014. Morphology of small, discontinuous montane meadow streams in the Sierra Nevada. *Geomorphology*, 219, 103-113.

Snaveley, N., Seitz, S. , & Szeliski, R. 2008. Modeling the world from internet photo collections. *International Journal of Computer Vision*, 802, 189-210.

Swanson, M., Kondolf, G., Boison, P., 1989. An example of rapid gully initiation and extension by subsurface erosion: Coastal San Mateo County, California – *Geomorphology* 2(4): 393-403.

Tetracam, <http://www.tetracam.com/>

Valentin, C., Poesen J., Yong Li, 2005. Gully Erosion: Impacts, Factors and Control. *Catena* vol. 63, 132–153.

Verhoeven, G. J. J., 2010. It's all about the format—unleashing the power of RAW aerial photography. *International Journal of Remote Sensing* 31, no. 8, 2009-2042.

Verhoeven, G. J., 2009. Providing an archaeological bird's-eye view—an overall picture of ground-based means to execute low-altitude aerial photography (LAAP) in Archaeology. *Archaeological Prospection*, 16(4), 233-249.

Verhoeven, G. J., Loenders, J., Vermeulen, F., & Docter, R., 2009. Helikite aerial photography—a versatile means of unmanned, radio controlled, low altitude aerial archaeology. *Archaeological Prospection*, 16(2), 125-138.

Verhoeven, G., 2008. Imaging the invisible using modified digital still cameras for straightforward and low-cost archaeological near-infrared photography. *Journal of Archaeological Science* 35, no. 12, 3087-3100.

Watts, A. C., Ambrosia, V. G., & Hinkley, E. A. 2012. Unmanned Aircraft Systems in Remote Sensing and Scientific Research: Classification and Considerations of Use. *Remote Sensing*, 1671-1692.

Wells, R., Momm H., Rigby, J., Bennett, S., Bingner, R., Dabney, S., 2013. An Empirical Investigation of Gully Widening Rates in Upland Concentrated Flows. *Catena* vol. 101, 114–121.

Westoby, M. , Brasington, J. , Glasser, N. , Hambrey, M. , & Reynolds, J., 2012. 'structure-from-motion' photogrammetry: A low-cost, effective tool for geoscience applications. *Geomorphology*, 179, 300-314.

Zongjian, L. I. N., 2008. UAV for mapping—low altitude photogrammetric survey. *International Archives of Photogrammetry and Remote Sensing*, Beijing, China.